Identifying PV Module Mismatch Faults by a Thermography-Based Temperature Distribution Analysis

Yihua Hu, *Member, IEEE*, Wenping Cao, *Senior Member, IEEE*, Jien Ma, Stephen J. Finney, and David Li

***Abstract*—Photovoltaic (PV) solar power generation is proven to be effective and sustainable but is currently hampered by relatively high costs and low conversion efficiency. This paper addresses both issues by presenting a low-cost and efficient temperature distribution analysis for identifying PV module mismatch faults by thermography. Mismatch faults reduce the power output and cause potential damage to PV cells. This paper first defines three fault categories in terms of fault levels, which lead to different terminal characteristics of the PV modules. The investigation of three faults is also conducted analytically and experimentally, and maintenance suggestions are also provided for different fault types. The proposed methodology is developed to combine the electrical and thermal characteristics of PV cells subjected to different fault mechanisms through simulation and experimental tests. Furthermore, the fault diagnosis method can be incorporated into the maximum power point tracking schemes to shift the operating point of the PV string. The developed technology has improved over the existing ones in locating the faulty cell by a thermal camera, providing a remedial measure, and maximizing the power output under faulty conditions.**

***Index Terms*—Degradation, fault diagnosis, photovoltaic (PV) power systems, temperature, thermography.**

I. Introduction

FOSSIL fuel-based electricity generation emits greenhouse gases, causes global warming, and is environmentally unsustainable. Renewable energy (e.g., solar, wind, geothermal, tidal, and wave), on the other hand, has received much attention and enormous research and development funding across the world over the years. Currently, grid-connected photovoltaic (PV) power is gaining popularity in the global renewables market, primarily owing to mass production of PV panels to reduce the capital costs and continuous improvement in power conversion technologies. However, current bottlenecks are still associated with high costs and low efficiency of PV systems. In addition to capital costs, the maintenance costs for PV panels are also high because they are generally installed in outdoor environments, and they are prone to various mechanical and electrical faults. These faults can result in additional power losses [1], hotspots [2], and different irradiances between PV modules [3]. These lead to loss of production and reduced generation efficiency. If left untreated, the faults may propagate to neighboring modules and cause a complete failure of the PV strings. The reliability, availability, and maintainability [4] of PVs have been a heated topic in research and application community [5] over the last three decades. In the literature, numerous diagnostic and monitoring methodologies have been proposed to minimize the outage period and to maximize the lifetime output of the PV systems [6]–[29].

II. Fault Mechanisms and Detection Methods

In general, there are three levels of faults developed in the PV systems, namely, cell, module, and string levels [6]. The cell faults include mechanical cracks, corrosion by water permeation, and material degradation by ultraviolet or thermal stress. The module faults are related to open circuits or short circuits resulting from the degeneration of the cells, cover, or sealant materials. The PV string faults consist of open circuits, short circuits, mismatch between PV modules, and partial shading. Mismatch faults are generally caused by encapsulant degradation, antireflection coating deterioration, manufacturing defects, and partial shading [30].

In a PV system, PV cells are connected in series to form a PV module, as shown in Fig. 1. A number of PV modules are then connected in series to form a PV string. Strings are further connected in parallel to form a PV array. This arrangement enables low dc voltage and current to be added up to a high output. For any solar power plants, the PV panels need to take up large space, which is likely to cause some nonuniform illumination when shadows or leaves cover part of the PV modules. This effect is termed partial shading [7]–[12].

If a PV array is under nonuniform illumination, the transferred electricity dramatically drops [7], [8], thus reducing the output power and generation efficiency. Under partial-shading conditions, mismatch faults cause overheating of some "faulted" cells/modules as well as multiple local maximum power points (MPPs). By developing analytical models of PVs, paper [13] simulates the electrical output characteristics of shadow-influenced PV arrays. The PV's current–voltage and power–voltage curves are characterized by multiple steps and peaks [13]. In practice, bypass diodes are generally added between the PV strings at the terminal to reduce the voltage

Manuscript received January 28, 2014; accepted August 4, 2014.

Y. Hu, S. J. Finney, and D. Li are with the Department of Electronic and Electrical Engineering, University of Strathclyde, Glasgow G1 1XW, U.K.

W. Cao is with the School of Electronics, Electrical Engineering and Computer Science, Queen's University Belfast, Belfast BT9 5BN, U.K.

J. Ma is with the College of Electrical Engineering, Zhejiang University, Hangzhou 310027, China.

Color versions of one or more of the figures in this paper are available online at http://ieeexplore.ieee.org.

Digital Object Identifier 10.1109/TDMR.2014.2348195

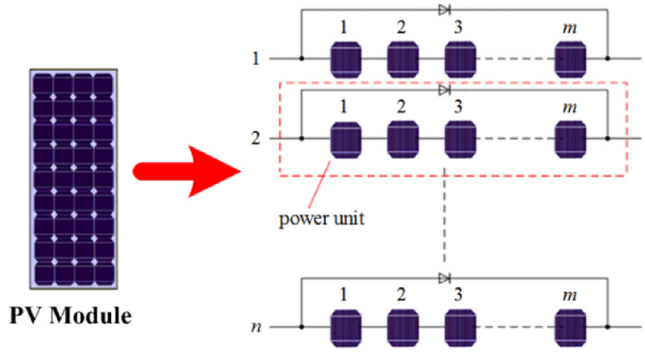

Fig. 1. Power units in a PV module.

imbalance [14]. Nonetheless, this causes difficulty in tracking the MPP [15]. As a consequence, when mismatch faults occur, conventional maximum power point tracking (MPPT) techniques become unsuitable to track the global MPP [16], [17]. Other tracking techniques such as particle swarm optimization [8], fuzzy logic [18], and power regulation [19] are devised to aid in this process. It is therefore important to develop a fault diagnostic system to detect any PV mismatch and to optimize the MPPT control accordingly. In the literature, common fault detection techniques include electrical (e.g., terminal measurements), visual (e.g., observing tarnish of cells and modules), and thermal approaches (e.g., spot heating). This paper attempts to improve energy efficiency and cost efficiency of PV systems by identifying mismatch faults and providing a remedial MPPT technique to suppress the mismatch, based on a temperature distribution analysis using a thermal camera.

Currently, thermal cameras are a useful tool for PV array fault diagnosis [20]–[29]. The health state of a grid-connected 20-kWp PV plant was investigated using a thermal camera [20]. It is effective in identifying breakdowns and hotspots but fails in distinguishing the different types of cell faults. Kaplani [21] studied the degradation of a PV system in the bus bars, contact solder bonds, blisters, and hotspots and also developed an algorithm to automatically differentiate faulty and healthy cells. Buerhopa *et al.* [22] reported the temperature differences for different faults such as bypassed substring, cell fracture, soldering, and shunted cell faults. Krenzinger and Andrade [24] investigated the thermal issues of the PV panel glass by developing an accurate temperature measurement method to offset reflection errors. Simon and Meyer [25] used infrared thermography to map the surface temperature distribution of a PV panel in a reverse bias mode in order to find the causes of localized heating. Kurnik *et al.* [26] derived an empirical coefficient for estimating the PV module temperature determined by analytical and experimental methods. However, in these papers, thermal cameras were only used independently to detect the temperature difference between cells or modules while captured image results are still open to human interpretation on whether or not the modules are faulty and how severe a fault may be.

In this study, thermal images are processed and input to a mathematical model for extracting quantitative information of a mismatch fault, which is then employed to regulate the MPPT control. This model combines electrical and thermal models through an energy balance based on a temperature distribution

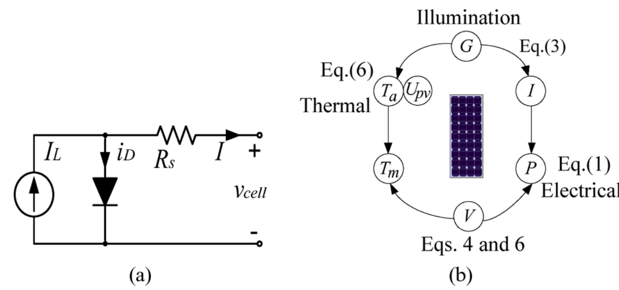

Fig. 2. Electrical and thermal characteristics of a PV cell. (a) Equivalent circuit [1]. (b) Energy balance.

analysis. After the temperature distribution characteristics are attained, the measured temperature difference can be evaluated, and a new MPPT scheme can be incorporated to minimize the impact of the occurred mismatch faults.

III. Modeling

When developing a parameter-based PV model, the electrical and thermal characteristics of the PV module should be included as they play an important role in the overall performance of PV systems. Fortunately, the electrical and thermal characteristics are interlinked through an energy balance that all receiving solar energy must be converted into electrical or heat energy.

A. Electrical Model

The electrical characteristic of a PV cell is influenced by both illumination and environmental temperature. The electrical model of a PV cell is generally represented by an equivalent circuit [see Fig. 2(a)] and is expressed by the following equations [10], [27]–[34]:

$$I = I_{\mathrm{L}} - I_{\mathrm{o}}\left[\exp\left(\frac{\varepsilon \cdot V}{T_m}\right) - 1\right] \quad (1)$$

$$\varepsilon = \frac{q}{N_s \cdot K \cdot A} \quad (2)$$

where

$$I_L = \frac{G}{G_{ref}}\left[I_{Lref} + k_i(T_m - T_{ref})\right] \quad (3)$$

$$I_o = I_{oref}\left(\frac{T_m}{T_{ref}}\right)^3 \exp\left[\frac{q \cdot E_{BG}}{N_s \cdot A \cdot K}\left(\frac{1}{T_{ref}} - \frac{1}{T_m}\right)\right] \quad (4)$$

where I is the PV module output current, I_L is the output current, q is the quantity of electric charge, A is the diode characteristic factor, K is the Boltzmann constant, I_o is the saturated current, T_m is the PV module temperature, G is the real irradiance of the PV cell, V is the output voltage, G_{ref} is the reference irradiance level (1000 W/m^2), I_{Lref} and I_{oref} are the reference values for I_L and I_o, and k_i is the current-temperature coefficient, normally provided by the manufacturer. T_{ref} is the reference temperature, N_s is the number of series-connected cells, and T_m is the PV module temperature. ε is a constant depending on q, N_s, K, A, and is calculated by the following equation:

$$I_{sc\_ref} - I_{mpp\_ref} = \frac{I_{sc\_ref}}{\exp\left(\frac{\varepsilon \cdot V_{oc\_ref}}{T_{ref}}\right) - 1}\left[\exp\left(\frac{\varepsilon \cdot V_{mpp\_ref}}{T_{ref}}\right) - 1\right] \quad (5)$$

where I_{mpp_ref}, I_{sc_ref}, and V_{oc_ref} are the MPP current, short-circuit current, and open-circuit voltage at a reference condition defined by the relevant standard.

B. Energy Balance

Energy balance can link electrical with thermal circuits based on two assumptions [32]: 1) the temperature difference between the PV cell and cover glass is neglected; 2) the cell temperature is uniform in a healthy module.

Therefore, the steady-state energy balance in PVs is given by

$$G \cdot A_m = V \cdot I + U_{pv} \cdot A_m(T_m - T_a) \quad (6)$$

where T_a is the ambient temperature, U_{pv} is an overall heat exchange coefficient from the module to ambient, and A_m is the PV panel area.

Equations (1) and (6) describe the electrical and thermal models, respectively, using main parameters such as I, V, T_m, G, U_{pv}, and T_a. Fig. 2(b) further illustrates the multiphysics loop of the energy balance in the PV system. The electrical parameters are mainly influenced by the effective solar energy S and module temperature T_m, whereas the thermal parameters are influenced by electrical power E and effective solar illumination G. Given a value of S, T_m depends on the electrical power of the PV module. As a result, this parameter-based model can be used to investigate the temperature difference upon a PV module fault.

IV. Temperature Distribution Analysis

When a mismatch fault occurs in the PV array, a temperature difference between the healthy and an unhealthy module is created, similar to partial shading observed from the terminal. Consequently, excessive heat and thermal stress can result in cell cracks. If the cell temperature exceeds its critical temperature, the delamination of cell encapsulants may occur. If the reverse bias exceeds the cell's breakdown voltage, the cell will be damaged [30]. In terms of the severity of mismatch faults, this paper defines three categories, namely, minor, medium, and heavy faults. Their terminal characteristics are different in the following aspects.

(i) Under a minor fault, the faulted power unit in the PV panel can still operate to generate electricity. As illustrated by the single arrow in Fig. 3(a), the current still passes through the PV cell string to generate an output. In this case, the faulty cell becomes an electrical load, powered by the healthy ones.

(ii) Under a medium fault, PV cells in the string are characterized by varying illumination levels. As presented in Fig. 3(b), the faulted cells can still operate as a source with a reduced power output. Because of the nonuniform illumination, the actual working point of the power unit is dictated by the operating point of the PV array.

(iii) Under a heavy-fault condition, the whole PV string is out of function while the bypass diode conducts to transmit the current, as indicated by the dotted arrow in Fig. 3(a). In essence, all PV cells in the string are open circuited.

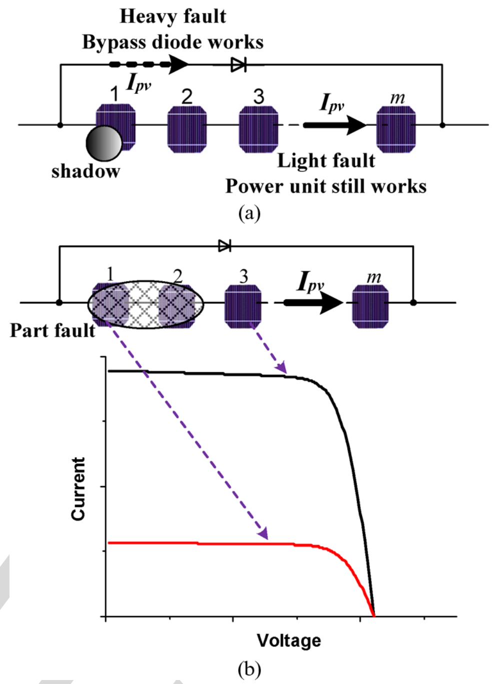

Fig. 3. Three categories of mismatch faults defined for a PV system. (a) Minor- and heavy-fault conditions. (b) Medium-fault condition.

If there exists a meaningful temperature difference, hotspot suppression is needed to shift the system MPP and to minimize the impact of the mismatch fault [35].

A. Analysis of Minor Faults

A temperature profile of the PV array under minor-fault conditions is presented in Fig. 4(a). The array is composed of b rows and a columns of PV modules where Module 21 is faulted. I_{array} and V_{array} are the current and voltage of the PV array, respectively. I_H and I_f are the currents of healthy and faulty strings, respectively. V_H is the module voltage of a healthy string, $V_{H'}$ is the voltage of the healthy module in the faulty string, T_H is the module temperature of a healthy string, $T_{H'}$ is the healthy module temperature within a faulted string, and T_f is the healthy cell temperature in a faulty power unit.

Under a minor-fault condition, the faulty PV cell cannot generate electricity and becomes a resistive load (R_{eq}). Owing to the series connection structure, the healthy cells supply power to the faulty PV cells (released as heat) and then create some hotspots. An equivalent circuit of the PV array is presented in Fig. 4(b), where V_{sf} stands for the voltage generated by the healthy PV cells in a faulty PV string, and R_{load} is the load resistance.

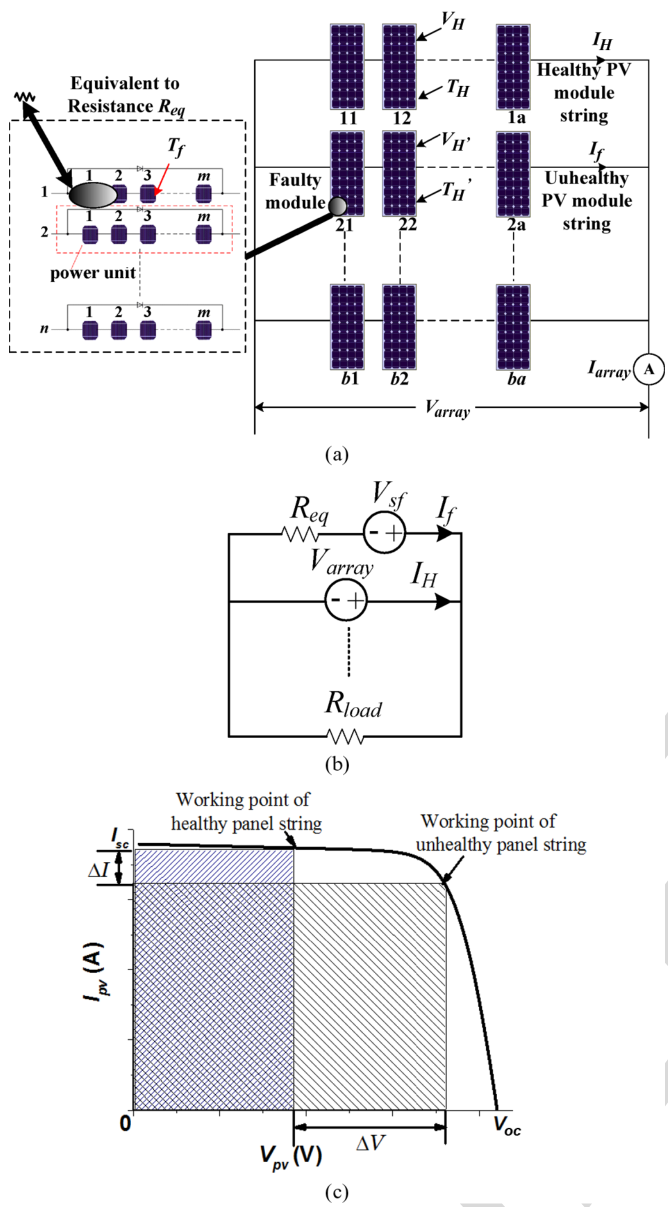

Fig. 4. PV system at a minor-fault condition. (a) PV array matrix. (b) Equivalent circuit upon a fault. (c) Shift of working points.

The electric characteristics of a faulty PV string are as follows:

$$V_{sf} - I_f R_{eq} = V_{array} \quad (7)$$

$$I_f = \frac{V_{sf}}{R_{eq} + R_{load}} \quad (8)$$

$$R_{eq} = \frac{V_{sf} - V_{array}}{I_f} \quad (9)$$

$$\Delta V = V_{H'} - V_H \quad (10)$$

$$\Delta I = I_H - I_f \quad (11)$$

$$I_f^2 \cdot R_{eq} < I_f (m - m_x) \frac{V_{H'}}{m \cdot n} \quad (12)$$

where ΔI is the current difference between the healthy and unhealthy strings, ΔV is the voltage difference between the healthy modules in healthy and unhealthy strings, and m_x is the number of faulty PV cells.

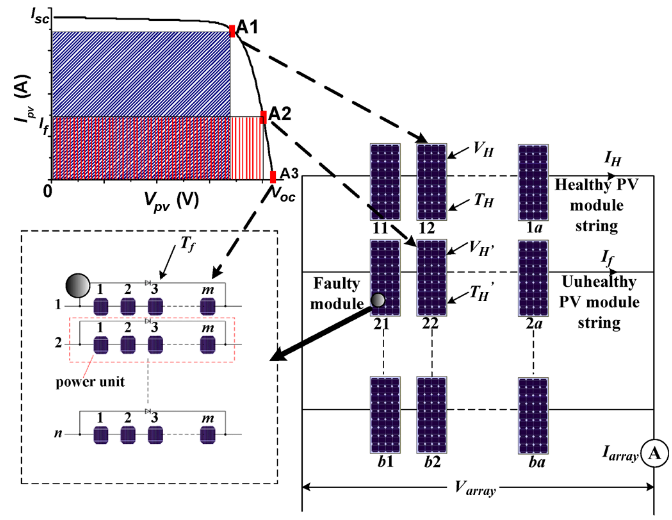

Fig. 5. PV system at a heavy-fault condition.

In Fig. 4(b), the voltage of a PV cell in a healthy string is lower than that of a healthy cell in a faulty string; the current of a PV cell in a healthy string is higher than that of a healthy cell in a faulty string. Equations (10)–(12) express the mathematical relationship for faulty and healthy PV strings. Equation (12) shows that when the output power of a faulted PV unit is higher than the I^2R power of its equivalent resistance, a minor fault is created, and hotspots begin to form on the fault cell.

Since the electrical power generated by healthy cells in the PV string supplies not only the load but also faulted cells (heating), the operating point in the current–voltage curve is effectively shifted. Fig. 4(c) demonstrates this in a PV system including healthy and unhealthy panel strings.

B. Analysis of Heavy Faults

Under a heavy-fault condition, the PV string containing the faulted cell/module loses production. Its operating points are illustrated in the output current–voltage curve in Fig. 5. Point A1 is the working point of the modules in the healthy string, A2 is the working point of the healthy modules in the faulty string, and A3 is the working point of healthy cells in the faulty module.

Because the faulty power unit is short-circuited by the bypass diode, the healthy cells in the faulty string are effectively open-circuited. The relative positions of A1, A2, and A3 are determined by the PV array structure and its electrical characteristics. Due to the antiparallel connection of the bypass diode, the faulty PV power unit is shorted by the diode. Therefore, its output voltage becomes zero. From (14), V_H is less than $V_{H'}$; I_H is greater than I_f, corresponding to working points A1 and A2. T_H and $T_{H'}$ depend on working points A1 and A2 in the curve. Because the faulty power unit is shorted by a bypass diode, the PV cells are open-circuited, corresponding to point A3. The output power of the faulted power unit is lower than the needed power of the equivalent resistance upon a fault; the power unit is shorted by the bypass diode.

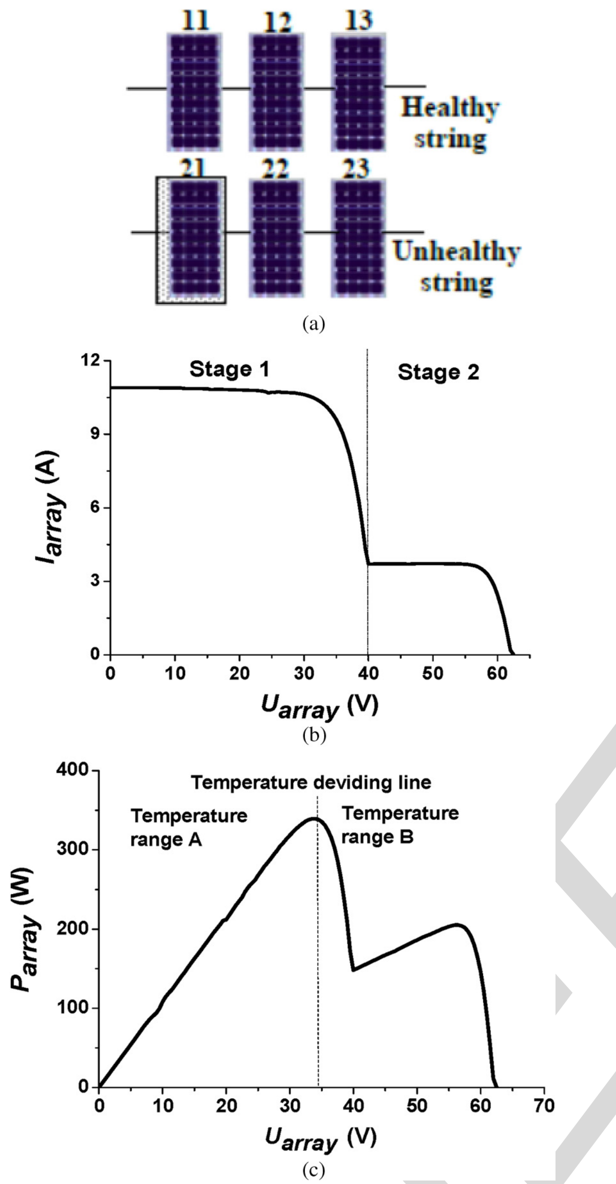

Fig. 6. PV system at a medium-fault condition. (a) Faulted module in a PV array. (b) Voltage–current curve of the faulted PV string. (c) Power–voltage curve of the faulted PV string.

V_H and $V_{H'}$ are thus given by

$$V_H = \frac{V_{array}}{a} \tag{13}$$

$$V_{H'} = \frac{V_H \cdot a \cdot n}{a \cdot n - n_x} \tag{14}$$

where n_x is the number of faulty power units in the faulty PV panel string, which can be identified by thermal cameras.

C. Analysis of Medium Faults

The operating point of the PV array strongly affects the condition of the healthy PV modules in the healthy string and sometimes in the fault string. Fig. 6(a) shows a 2 × 3 PV array under a medium fault, where module 21 is a faulted PV module,

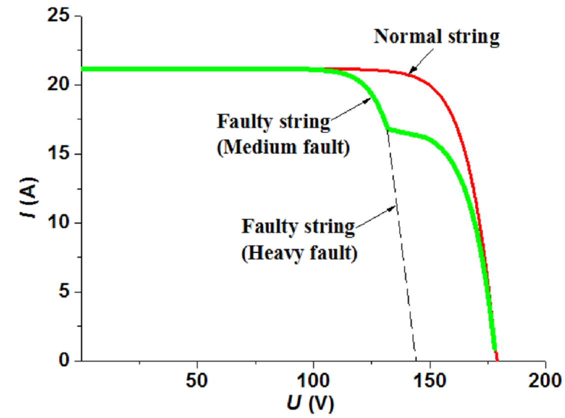

Fig. 7. Difference between medium and heavy faults.

and the rest of PV modules are healthy. Compared with other PV module (1000 W/m^2), No. 21 has the lower illumination (300 W/m^2). Fig. 6(b) and (c) presents the current–voltage and power–voltage curves, respectively, obtained from simulation.

In Fig. 6(b), the current–voltage curve of the PV array has a multistage feature, and the power–voltage curve has thus multiple MPPs. Two stages are identified in this figure. In Fig. 6(c), there exists a temperature dividing line in the power–voltage curve, separating two temperature ranges.

When the PV array works at stage 1, the current is between 4.5 and 10.8 A, and the corresponding voltage is 0–40 V. Both healthy and unhealthy strings can generate electricity. Since there are two healthy modules in the faulted string, they collectively provide an output voltage of 0–40 V. In the temperature range A, the temperature of modules 22 and 23 is lower than that of modules 11–13. According to the electrical and thermal balance equations, the output electrical power of the healthy modules in the faulty sting is higher than that of the healthy string. The corresponding temperature of the PV modules in the faulted string is lower than that in the healthy string.

While the PV array works at stage 2, the current is 0–4.5 A, and the corresponding voltage is 40–62 V. In this case, only the healthy string can generate electricity. The faulty string is shorted by the bypass diode, and the healthy module in the faulted string is in open circuit. In effect, all the effective solar energy is transferred into heat. In temperature range B, the faulted string has a higher temperature than the healthy string, indicating a different temperature characteristic to range A.

D. Terminal Characteristics of the Three Mismatch Faults

Based on a thermal image, PV array current and voltage information, three mismatch faults can be clearly identified.

A minor fault will cause hotspots characterized by a small faulty cell area (e.g., bird drops or leaves). When this fault occurs, it is easy to clear but often needs human intervention.

A medium fault and a heavy fault are both caused by nonuniform illumination. For the medium fault, the faulty PV string can still generate a high voltage output (140–180 V in Fig. 7). In the high-voltage region, the output current in the faulty string

TABLE I
SPECIFICATIONS OF THE EQUIPMENT

Item	Parameter	Value
PV Module	Open-circuit voltage	21.8 V
	Short-circuit current	6.23 A
	Power output	100 W
	MPP current	5.69 A
	MPP voltage	17 V
	Current temperature coefficient	0.06%/K
	Voltage temperature coefficient	–0.36%/K
	Power temperature coefficient	–0.45%/K
	NOCT	46±2
Thermal camera	Type	FLUKE Ti10
	IR resolution	160×120 pixels
	Thermal sensitivity (NETD)	< 0.13°C/130 mK
	Minimum focus distance	15 cm
	Spatial resolution (IFOV)	2.5 mRad
	Image frequency	9 Hz
	Accuracy	±2°C or 2%

is significantly lower than normal strings, whereas for the heavy fault, the faulty PV string is shorted so that it cannot generate any output. Therefore, the high-voltage region (140–180 V) is absent from the output curve in Fig. 7. Clearly, the medium and heavy faults can be easily distinguished. The medium and heavy faults would not cause an immediate damage to the PV module but can cause nonuniform aging and long-term damage to PV modules if left untreated.

V. EXPERIMENTAL TESTS

A PV experimental platform is developed using six PV panels arranged into two strings, with each having three series-connected PV panels, which are made of polysilicon and whose specifications are given in Table I. The PV panels' surface temperature is recorded by a *Fluke* thermal camera whose specifications are also listed in Table I.

The thermal camera can record a color image in varying intensities and send it to a central computer. In order to analyze the thermal feature of the device under test, the thermography of each PV panel is extracted by freehand cropping in a MATLAB program and is then used to calculate its relative temperature with a reference. Although the absolute accuracy of the thermal camera is only ±2 °C, its sensitivity is better than 0.1 °C. In this work, the proposed fault category analysis is based on identifying the temperature difference in the thermal image of the PV module and is thus effective.

Without a doubt, the use of thermal camera can help locate the faulty cells instantly and guide the maintenance work to conduct according to the type of occurred faults.

A. Tests Under a Minor Fault

Two parallel diodes are connected in the junction box, as shown in Fig. 8(a). One of the power units is connected with a resistance, and the other was made open-circuited to testify the temperature characteristics under different load conditions. Thus, there are two power units in all PV modules, each containing 18 PV cells.

The corresponding thermal image is presented in Fig. 8(b). The power unit A temperature is 32.6 °C, and the power unit B temperature is 36.1 °C. Because some of the solar energy in unit A is converted into electricity, its surface temperature is lower than that of unit B, in which all of the solar energy is transferred into heat.

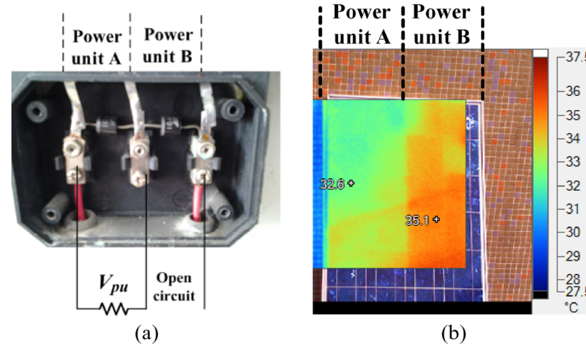

Fig. 8. Photos of the PV module. (a) Terminal connection. (b) Thermal image.

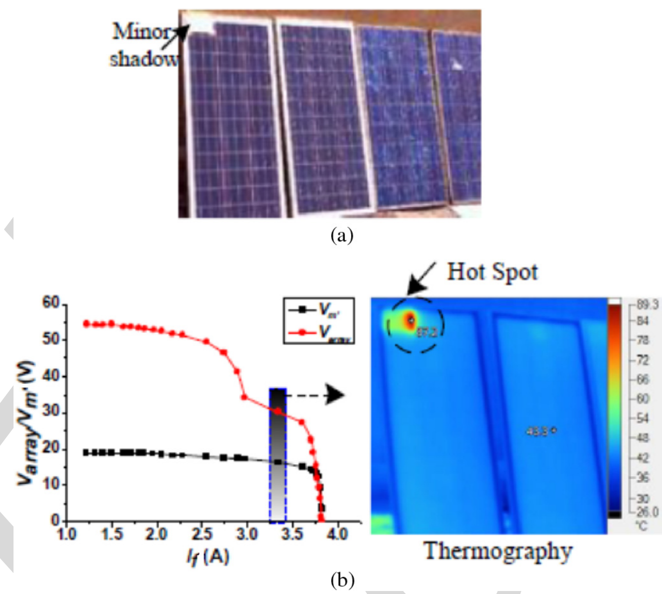

Fig. 9. Tests at a minor-fault condition. (a) Experimental scene to simulate minor shadowing. (b) Output characteristics and thermography.

Three PV panels are then connected in series, and one is covered by opaque materials to emulate partial shading. As shown in Fig. 9, a hotspot is recorded by thermography at the location of partial shading, and its I–V curve is shifted as well. A further experiment is carried out under 820-W/m^2 illumination at 25 °C ambient temperature. The terminal voltage is recorded 16 V from the faulty PV panel and 14 V from the two healthy panels. Because this is a minor shadow test, the healthy cells in the faulty string have a higher output voltage, and the faulted cell is equivalent to a resistance, raising the output voltage of the PV string under a minor-fault condition. From measurements, the voltage of the faulty PV cell is 9 V, and its equivalent resistance is 2.64 Ω. The electrical heating power for the faulty PV cell is 30.52 W, and the solar energy in the hotspot area is 15.5 W. According to the thermography measurement, the hotspot temperature reaches 87.2 °C, whereas the temperature of the healthy PV cells is only 44.3 °C. These are coincided with the theory analysis.

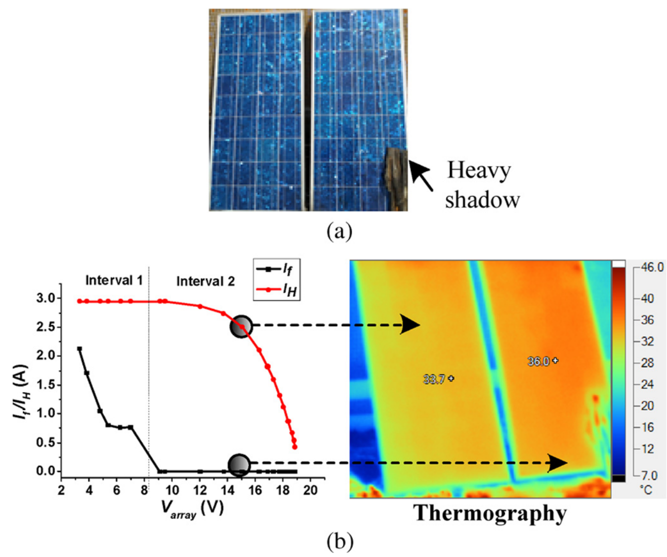

Fig. 10. Tests at a heavy-fault condition. (a) Experimental scene to simulate heavy shadowing. (b) Output characteristics and thermography.

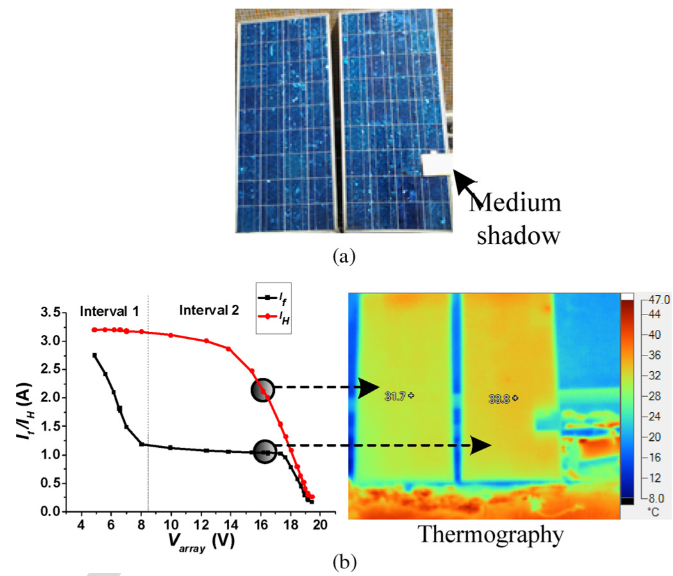

Fig. 11. Tests at a medium-fault condition. (a) Experimental scene to simulate medium shadowing. (b) Output characteristics and thermography.

B. Tests Under a Heavy Fault

Next, three PV cells are all covered up to create a heavy-fault condition, as shown in Fig. 10. Compared with the minor-fault scenario, the covered area is greater so that the faulted power unit is shorted by the bypass diode. The experiment is conducted under an illumination of 690 W/m^2 at 24 °C. The average temperature of the healthy PV panel is 33.7 °C, whereas the average temperature of the unhealthy PV module is 36.0 °C. The faulty PV panel is shorted by bypass diodes, and all the solar energy is converted into heat. However, the healthy PV panels are still capable of converting some of incoming solar energy into electricity, leading to a lower panel temperature. In Fig. 10, there is no current flowing at the faulted module during interval 2. Its current gradually increases during interval 1 because the faulty PV module is shorted by the bypass diode.

C. Tests Under a Medium Fault

In this test, one PV module is partially covered up by a thin paper to represent a medium-fault condition (e.g., partial shading), as shown in Fig. 11. The reason for using a thin paper is to ensure that some illumination can penetrate into the shaded cells through the paper. In the previous cases, light penetration is almost completely stopped.

The experiment is carried out under an illumination of 740 W/m^2 at 22 °C. The faulty power unit output is influenced by the unhealthy PV cells. The average temperature of a healthy PV panel is 31.7 °C, whereas that of the unhealthy PV module is recorded 33.8 °C. In interval 1, the faulty power unit is shorted by the bypass diode because the faulty power unit cannot generate a higher enough current to support load.

D. Tests Under Different Operating Points

Further tests are conducted to investigate the impact of the operating points, under a heavy-fault condition.

Fig. 12(a) shows the photo of a 2 × 3 PV array employed in this experiment. Fig. 12(b) and (c) depicts the output curves of the tested PV array. Fig. 12(d) shows a thermal image at working point A (with an array output voltage of 34 V). As discussed in Section III, the working point can cause the temperature difference. However, in this case, the two healthy modules in the fault string operate at 17 V, which is close to the MPP voltage. The corresponding temperatures are 19.9 °C and 19.8 °C, respectively, almost undistinguishable. The modules' output voltage in healthy string is 11.3 V, and the corresponding temperatures are 20.9 °C, 20.9 °C, and 21 °C for the three panels. At working point A, the module temperature in the healthy string is higher than the healthy module in the fault string. Fig. 12(e) shows a thermal image at working point B at the array output voltage 52 V. The output voltage of the healthy module is 17.3 V, which is close to MPP voltage, whereas the voltages of modules No. 22 and No. 23 are close to the open-circuit voltage, suggesting more energy is converted into heat. By the thermography measurement, the temperatures of healthy modules are 19.6 °C, 19.7 °C, and 19.7 °C, whereas the temperatures of healthy modules in the faulty string are both 21.6 °C. The temperature difference coincides with the theoretical analysis.

By the above analysis, it is clear that the temperatures of the healthy modules in both the healthy string and the unhealthy string are changed with the PV array output voltage. As a consequence, it is of critical importance to adjust the operating points according to different fault conditions.

E. Tests Under Open- and Short-Circuit Faults

Fig. 13 further compares the temperature difference between an open-circuit and a short-circuit scenario. At an open-circuit condition, the temperature distribution within a PV string is uniform; the corresponding temperature is 11.3 °C. Under a short-circuit condition, the temperature becomes varied. The

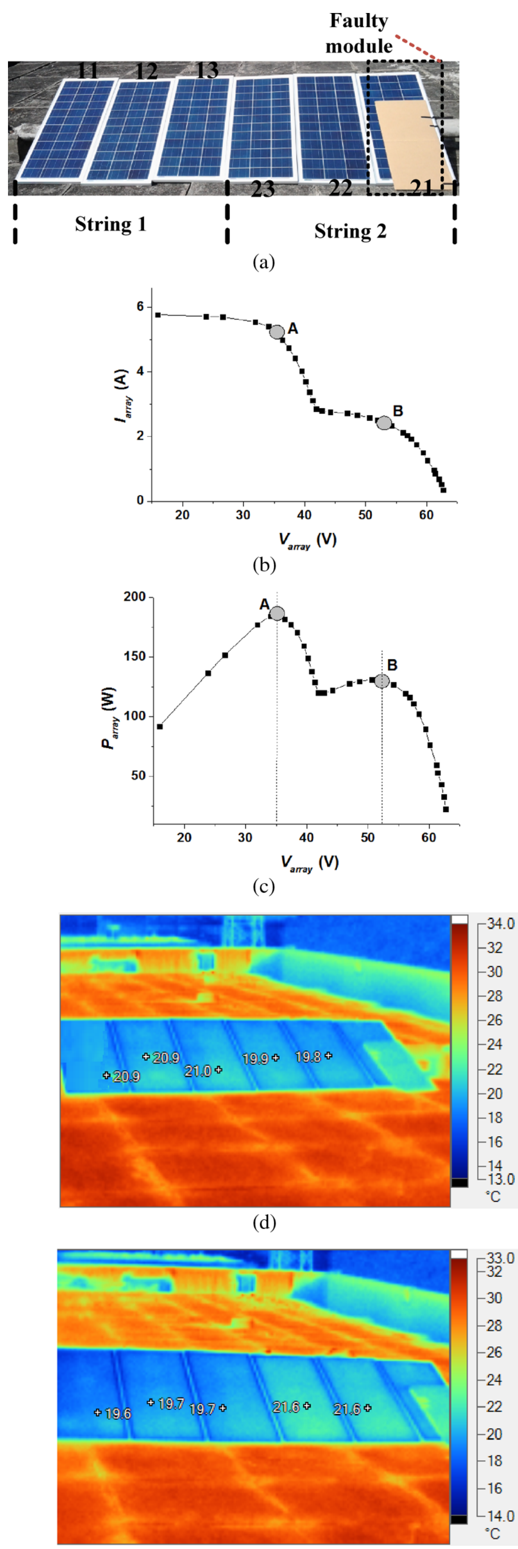

Fig. 12. Temperature distribution under two different operating points. (a) Tested PV panels. (b) Current–voltage curve. (c) Power–voltage curve. (d) Thermography at working point A. (e) Thermography at working point B.

temperatures of the faulty PV cells are 17.5 °C and 16.6 °C; the temperature of the healthy cells is 10.8 °C, which is even lower than that at the open-circuit condition. Under a short-circuit condition, the faulty PV cells have a higher equivalent resistance, thus shifting the working point of the healthy PV cells. The fault PV cell is heated up at the same time. Therefore, the healthy cells under a short-circuit fault have a lower temperature than that at an open-circuit fault.

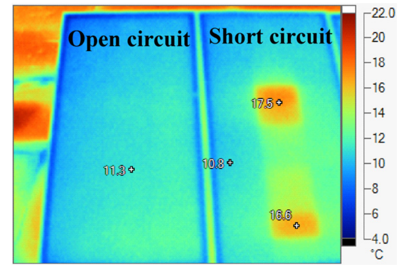

Fig. 13. Temperature difference between open and short circuits.

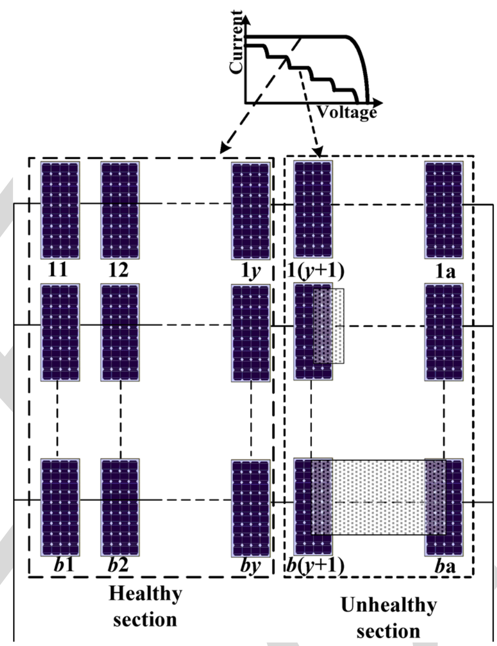

Fig. 14. Separation of healthy sections from fault PV arrays.

F. Assistance With MPPT Control

From the above analysis and experimental tests, the terminal characteristics and operating conditions of the PV module are known. The temperature distribution can then be input to the MPPT algorithm under mismatch fault conditions.

The maximum healthy section can be separated from fault PV arrays. As illustrated in Fig. 14, the whole PV array can be first divided into two sections: healthy and unhealthy. In the healthy section, all the modules in all strings are deemed to be fault free. That is, there is only an MPP in the section (local MPP). The global MPPT is effective to locate the first local MPP, significantly reducing the search range. In the unhealthy section where one or more modules are subject to shading, the temperature distribution of the faulty PV modules is then analyzed by thermography. As a result, the global MPP operating range can be directly located without much searching effort.

VI. Conclusion

Solar power is a cost-sensitive market. This work promotes its market acceptance by reducing the maintenance cost and improving the conversion efficiency of PV systems. This paper has presented a thermography-based temperature distribution analysis to analyze three different fault categories, and the proposed methodology was validated by both simulation and experimental test results. The proposed technology will lower the capital and operational costs of PV plants as well as increase their energy efficiency.

Compared with the existing methods, this work has made the following improvements.

(i) The thermal camera can help locate the faulty cells instantly and guide the maintenance work to conduct according to the type of occurred faults.

(ii) The temperature distributions under the PV fault conditions are analyzed by a new electrical–thermal model.

(iii) The mechanisms and impacts of three fault categories are defined and quantitatively studied. The mechanisms and difference of three faults is also illustrated.

(iv) The operating points of healthy and faulty PV arrays are described theoretically and experimentally, which could be used to improve the PV performance upon a mismatch fault.

(v) The thermography-based temperature distribution analysis is effective in establishing parameter-based models and developing an optimized global MPPT algorithm.

References

[1] A. Maki and S. Valkealahti, "Effect of photovoltaic generator components on the number of MPPs under partial shading conditions," *IEEE Trans. Energy Convers.*, vol. 28, no. 4, pp. 1008–1017, Dec. 2013.

[2] M. Z. S. El-Dein, M. Kazerani, and M. M. A. Salama, "Optimal photovoltaic array reconfiguration to reduce partial shading losses," *IEEE Trans. Sustainable Energy*, vol. 4, no. 1, pp. 145–153, Jan. 2013.

[3] E. V. Paraskevadaki and S. A. Papathanassiou, "Evaluation of MPP voltage and power of mc-Si PV modules in partial shading conditions," *IEEE Trans. Energy Convers.*, vol. 26, no. 3, pp. 923–932, Sep. 2011.

[4] H. A. Lauffenburger and R. T. Anderson, "Reliability terminology and formulae for photovoltaic power systems," *IEEE Trans. Rel.*, vol. R-31, no. 3, pp. 289–295, Aug. 1982.

[5] L. H. Stember, W. R. Huss, and M. S. Bridgman, "A methodology for photovoltaic system reliability and economic analysis," *IEEE Trans. Rel.*, vol. R-31, no. 3, pp. 296–303, Aug. 1982.

[6] T. Takashima, J. Yamaguchi, K. Otani, K. Kato, and M. Ishida, "Experimental studies of failure detection methods in PV module strings," in *Proc. 4th IEEE World Conf. Photovoltaic Energy Convers.*, 2006, vol. 2, pp. 2227–2230.

[7] Y. A. Mahmoud, W. Xiao, and H. H. Zeineldin, "A parameterization approach for enhancing PV model accuracy," *IEEE Trans. Ind. Electron.*, vol. 60, no. 12, pp. 5708–5716, Dec. 2013.

[8] Y. H. Liu, S. C. Huang, J. W. Huang, and W. C. Liang, "A particle swarm optimization-based maximum power point tracking algorithm for PV systems operating under partially shaded conditions," *IEEE Trans. Energy Convers.*, vol. 27, no. 4, pp. 1027–1035, Dec. 2012.

[9] K. Ding, X. Bian, H. Liu, and T. Peng, "A MATLAB–Simulink-based PV module model and its application under conditions of nonuniform irradiance," *IEEE Trans. Energy Convers.*, vol. 27, no. 4, pp. 864–872, Dec. 2012.

[10] A. Mäki and S. Valkealahti, "Power losses in long string and parallel-connected short strings of series-connected silicon-based photovoltaic modules due to partial shading conditions," *IEEE Trans. Energy Convers.*, vol. 27, no. 1, pp. 173–183, Mar. 2012.

[11] T. Takashima *et al.*, "Experimental studies of fault location in PV module strings," *Sol. Energy Mater. Sol. Cells*, vol. 93, no. 6/7, pp. 1079–1082, Jun. 2009.

[12] H. Patel and V. Agarwal, "MATLAB-based modeling to study the effects of partial shading on PV array characteristics," *IEEE Trans. Energy Convers.*, vol. 23, no. 1, pp. 302–310, Mar. 2008.

[13] H. Patel and V. Agarwal, "Maximum power point tracking scheme for PV systems operating under partially shaded conditions," *IEEE Trans. Ind. Electron.*, vol. 55, no. 4, pp. 1689–1698, Apr. 2008.

[14] H. Ziar, M. Nouri, B. Asaei, and S. Farhangi, "Analysis of overcurrent occurrence in photovoltaic modules with overlapped by-pass diodes at partial shading," *IEEE J. Photovoltaics*, vol. 4, no. 2, pp. 713–721, Mar. 2014.

[15] A. Bidram, A. Davoudi, and R. S. Balog, "Control and circuit techniques to mitigate partial shading effects in photovoltaic arrays," *IEEE J. Photovoltaics*, vol. 2, no. 4, pp. 532–546, Oct. 2012.

[16] E. I. Batzelis, I. A. Routsolias, and S. A. Papathanassiou, "An explicit PV string model based on the Lambert W function and simplified MPP expressions for operation under partial shading," *IEEE Trans. Sustainable Energy*, vol. 5, no. 1, pp. 301–312, Jan. 2014.

[17] E. Karatepe and T. Hiyama, "Simple and high-efficiency photovoltaic system under non-uniform operating conditions," *IET Renew. Power Gen.*, vol. 4, no. 4, pp. 354–368, Jul. 2010.

[18] B. N. Alajmi, K. H. Ahmed, S. J. Finney, and B. W. Williams, "Maximum power point tracking technique for partially shaded photovoltaic systems in microgrids," *IEEE Trans. Ind. Electron.*, vol. 60, no. 4, pp. 1596–1606, Apr. 2013.

[19] L. F. L.Villa, T. P. Ho, J. C. Crebier, and B. Raison, "A power electronics equalizer application for partially shaded photovoltaic modules," *IEEE Trans. Ind. Electron.*, vol. 60, no. 3, pp. 1179–1190, Mar. 2013.

[20] G. Acciani, G. B. Simione, and S. Vergura, "Thermographic analysis of photovoltaic panels," in *Proc. ICREPQ*, Granada, Spain, 2010, pp. 1–3.

[21] E. Kaplani, "Detection of degradation effects in field-aged c-Si solar cells through IR thermography and digital image processing," *Int. J. Photoenergy*, vol. 2012, pp. 396 792-1–396 792-11, 2012.

[22] C. L. Buerhopa *et al.*, "Reliability of IR-imaging of PV-plants under operating conditions," *Sol. Energy Mater. Sol. Cells*, vol. 107, pp. 154–164, Dec. 2012.

[23] P. Parinya, B. Wiengmoon, D. Chenvidhya, and C. Jivacate, "Comparative study of solar cells characteristics by temperature measurement," in *Proc. 22nd Eur. Photovoltaic Sol. Energy Conf.*, Milan, Italy, 2007, pp. 2775–2778.

[24] A. Krenzinger and A. C. Andrade, "Accurate outdoor glass thermographic thermometry applied to solar energy devices," *Sol. Energy*, vol. 81, no. 8, pp. 1025–1034, Aug. 2007.

[25] M. Simon and E. L. Meyer, "Detection and analysis of hot-spot formation in solar cells," *Sol. Energy Mater. Sol. Cells*, vol. 94, no. 2, pp. 106–113, Feb. 2010.

[26] J. Kurnik, M. Jankovec, K. Brecl, and M. Topic, "Outdoor testing of PV module temperature and performance under different mounting and operational conditions," *Sol. Energy Mater. Sol. Cells*, vol. 95, no. 1, pp. 373–376, Jan. 2011.

[27] G. Farivar and B. Asaei, "A new approach for solar module temperature estimation using the simple diode model," *IEEE Trans. Energy Convers.*, vol. 26, no. 4, pp. 1118–1126, Dec. 2011.

[28] M. U. Siddiqui, A. F. M. Arif, L. Kelley, and S. Dubowsky, "Three-dimensional thermal modeling of a photovoltaic module under varying conditions," *Sol. Energy*, vol. 86, no. 9, pp. 2620–2631, Sep. 2012.

[29] H. F. Tsai and H. L. Tsai, "Implementation and verification of integrated thermal and electrical models for commercial PV modules," *Sol. Energy*, vol. 86, no. 1, pp. 654–665, Jan. 2012.

[30] E. L. Meyer and E. E. van Dyk, "Assessing the reliability and degradation of photovoltaic module performance parameters," *IEEE Trans. Rel.*, vol. 53, no. 1, pp. 83–92, Mar. 2004.

[31] A. Chatterjee, A. Keyhani, and D. Kapoor, "Identification of photovoltaic source models," *IEEE Trans. Energy Convers.*, vol. 26, no. 3, pp. 883–889, Sep. 2011.

[32] M. Mattei, G. Notton, C. Cristofari, M. Muselli, and P. Poggi, "Calculation of the polycrystalline PV module temperature using a simple method of energy balance," *Renew. Energy*, vol. 31, no. 4, pp. 553–567, Apr. 2006. **AQ1**

[33] A. Luque, G. Sala, and J. C. Arboiro, "Electric and thermal model for non-uniformly illuminated concentration cells," *Sol. Energy Mater. Sol. Cells*, vol. 51, no. 3/4, pp. 269–290, Feb. 1998.

[34] Y. Hu *et al.*, "Photovoltaic fault detection using a parameter based model," *Sol. Energy*, vol. 96, pp. 96–10, Oct. 2013.

[35] S. A. Spanoche, J. D. Stewart, S. L. Hawley, and I. E. Opris, "Model-based method for partially shaded PV module hot-spot suppression," *IEEE J. Photovoltaics*, vol. 3, no. 2, pp. 785–790, Apr. 2013.

Yihua Hu (M'13) received the B.S. degree in electrical motor drives and the Ph.D. degree in power electronics and drives from China University of Mining and Technology, Jiangsu, China, in 2003 and 2011, respectively.

Between 2011 and 2013, he was a Postdoctoral Fellow with the College of Electrical Engineering, Zhejiang University, Hangzhou, China. Between November 2012 and February 2013, he was an academic Visiting Scholar with the School of Electrical and Electronic Engineering, Newcastle University, Newcastle upon Tyne, U.K. He is currently a Research Associate with the Department of Electronic and Electrical Engineering, University of Strathclyde, Glasgow, U.K. His research interests include photovoltaic generation systems, dc–dc/dc–ac converters, and electrical motor drives.

Wenping Cao (M'05–SM'11) received the B.Eng. degree in electrical engineering from Beijing Jiaotong University, Beijing, China, in 1991 and the Ph.D. degree in electrical machines and drives from the University of Nottingham, Nottingham, U.K., in 2004.

He is currently a Senior Lecturer with Queen's University Belfast, Belfast, U.K. His research interests include thermal performance of electric machines, drives, and power electronics.

Dr. Cao was a recipient of the Best Paper Award at the LDIA'13 Conference. He serves as an Associate Editor for the IEEE TRANSACTIONS ON INDUSTRY APPLICATIONS, the *IEEE Industry Applications Magazine*, the *IET Power Electronics*, and nine other international journals. He is also a member of the Institution of Engineering and Technology and a Fellow of Higher Education Academy.

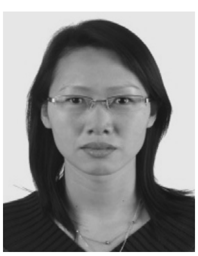

Jien Ma received the B.Eng. degree in mechatronics from Yanshan University, Qinhuangdao, China, in 2003 and the Ph.D. degree in electromechanics from Zhejiang University, Hangzhou, China, in 2009.

She is currently a Lecturer with the College of Electrical Engineering, Zhejiang University. Her interests include electrical machines and drives, including permanent-magnet machines and cooling system design, mechatronics machines, and magneto fluid bearings.

Stephen J. Finney received the M.Eng. degree in electrical and electronic engineering from Loughborough University of Technology, Loughborough, U.K., in 1988 and the Ph.D. degree from Heriot-Watt University, Edinburgh, U.K., in 1995.

Prior to joining the Power Electronics Research Group at Heriot-Watt University in 1990, he was with the Electricity Council Research Centre. From 1994 to 2005, he was a member of the academic staff with Heriot-Watt University. Since 2005, he has been with the Institute of Energy and Environment, University of Strathclyde, Glasgow, U.K., where he is currently a Professor, specializing in power electronic systems. His research interests include power electronics for high-power applications and the use of power electronics for power transmission and distribution.

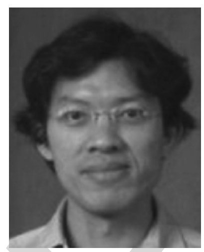

David Li received the Ph.D. degree in electrical engineering from National Taiwan University, Taipei, Taiwan, in 2001.

He then joined the Industrial Technology Research Institute, Taiwan, and the University of Edinburgh, Edinburgh, U.K., working on optical communications and optoelectronics. Since January 2014, he has been a Senior Lecturer with the Centre for Biophotonics, University of Strathclyde, Glasgow, U.K. His current research interests include solid-state cameras, embedded systems, digital signal processing, mixed-signal integrated circuit design, fluorescence-based sensing and imaging systems, electrical impedance sensing systems, forward models of electrical impedance tomography, and finite-element/finite-difference and numerical modeling.

AUTHOR QUERIES

AUTHOR PLEASE ANSWER ALL QUERIES

AQ1 = Note that references [32] and [35] are the same. Therefore, reference [35] was deleted from the list. Citations were renumbered accordingly. Please check.

END OF ALL QUERIES

Identifying PV Module Mismatch Faults by a Thermography-Based Temperature Distribution Analysis

Yihua Hu, *Member, IEEE*, Wenping Cao, *Senior Member, IEEE*, Jien Ma, Stephen J. Finney, and David Li

***Abstract*—Photovoltaic (PV) solar power generation is proven to be effective and sustainable but is currently hampered by relatively high costs and low conversion efficiency. This paper addresses both issues by presenting a low-cost and efficient temperature distribution analysis for identifying PV module mismatch faults by thermography. Mismatch faults reduce the power output and cause potential damage to PV cells. This paper first defines three fault categories in terms of fault levels, which lead to different terminal characteristics of the PV modules. The investigation of three faults is also conducted analytically and experimentally, and maintenance suggestions are also provided for different fault types. The proposed methodology is developed to combine the electrical and thermal characteristics of PV cells subjected to different fault mechanisms through simulation and experimental tests. Furthermore, the fault diagnosis method can be incorporated into the maximum power point tracking schemes to shift the operating point of the PV string. The developed technology has improved over the existing ones in locating the faulty cell by a thermal camera, providing a remedial measure, and maximizing the power output under faulty conditions.**

***Index Terms*—Degradation, fault diagnosis, photovoltaic (PV) power systems, temperature, thermography.**

I. Introduction

FOSSIL fuel-based electricity generation emits greenhouse gases, causes global warming, and is environmentally unsustainable. Renewable energy (e.g., solar, wind, geothermal, tidal, and wave), on the other hand, has received much attention and enormous research and development funding across the world over the years. Currently, grid-connected photovoltaic (PV) power is gaining popularity in the global renewables market, primarily owing to mass production of PV panels to reduce the capital costs and continuous improvement in power conversion technologies. However, current bottlenecks are still associated with high costs and low efficiency of PV systems. In addition to capital costs, the maintenance costs for PV panels are also high because they are generally installed in outdoor environments, and they are prone to various mechanical and electrical faults. These faults can result in additional power losses [1], hotspots [2], and different irradiances between PV modules [3]. These lead to loss of production and reduced generation efficiency. If left untreated, the faults may propagate to neighboring modules and cause a complete failure of the PV strings. The reliability, availability, and maintainability [4] of PVs have been a heated topic in research and application community [5] over the last three decades. In the literature, numerous diagnostic and monitoring methodologies have been proposed to minimize the outage period and to maximize the lifetime output of the PV systems [6]–[29].

II. Fault Mechanisms and Detection Methods

In general, there are three levels of faults developed in the PV systems, namely, cell, module, and string levels [6]. The cell faults include mechanical cracks, corrosion by water permeation, and material degradation by ultraviolet or thermal stress. The module faults are related to open circuits or short circuits resulting from the degeneration of the cells, cover, or sealant materials. The PV string faults consist of open circuits, short circuits, mismatch between PV modules, and partial shading. Mismatch faults are generally caused by encapsulant degradation, antireflection coating deterioration, manufacturing defects, and partial shading [30].

In a PV system, PV cells are connected in series to form a PV module, as shown in Fig. 1. A number of PV modules are then connected in series to form a PV string. Strings are further connected in parallel to form a PV array. This arrangement enables low dc voltage and current to be added up to a high output. For any solar power plants, the PV panels need to take up large space, which is likely to cause some nonuniform illumination when shadows or leaves cover part of the PV modules. This effect is termed partial shading [7]–[12].

If a PV array is under nonuniform illumination, the transferred electricity dramatically drops [7], [8], thus reducing the output power and generation efficiency. Under partial-shading conditions, mismatch faults cause overheating of some "faulted" cells/modules as well as multiple local maximum power points (MPPs). By developing analytical models of PVs, paper [13] simulates the electrical output characteristics of shadow-influenced PV arrays. The PV's current–voltage and power–voltage curves are characterized by multiple steps and peaks [13]. In practice, bypass diodes are generally added between the PV strings at the terminal to reduce the voltage

Manuscript received January 28, 2014; accepted August 4, 2014.
Y. Hu, S. J. Finney, and D. Li are with the Department of Electronic and Electrical Engineering, University of Strathclyde, Glasgow G1 1XW, U.K.
W. Cao is with the School of Electronics, Electrical Engineering and Computer Science, Queen's University Belfast, Belfast BT9 5BN, U.K.
J. Ma is with the College of Electrical Engineering, Zhejiang University, Hangzhou 310027, China.
Color versions of one or more of the figures in this paper are available online at http://ieeexplore.ieee.org.
Digital Object Identifier 10.1109/TDMR.2014.2348195

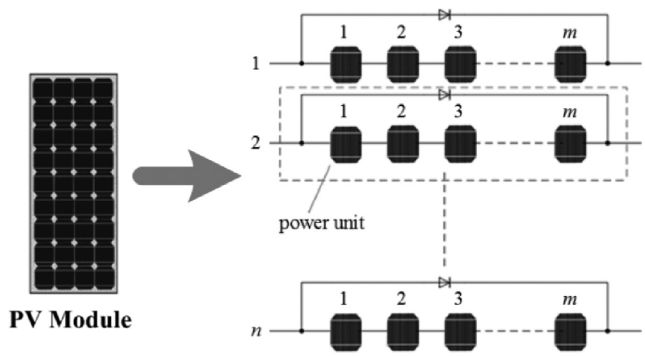

Fig. 1. Power units in a PV module.

imbalance [14]. Nonetheless, this causes difficulty in tracking the MPP [15]. As a consequence, when mismatch faults occur, conventional maximum power point tracking (MPPT) techniques become unsuitable to track the global MPP [16], [17]. Other tracking techniques such as particle swarm optimization [8], fuzzy logic [18], and power regulation [19] are devised to aid in this process. It is therefore important to develop a fault diagnostic system to detect any PV mismatch and to optimize the MPPT control accordingly. In the literature, common fault detection techniques include electrical (e.g., terminal measurements), visual (e.g., observing tarnish of cells and modules), and thermal approaches (e.g., spot heating). This paper attempts to improve energy efficiency and cost efficiency of PV systems by identifying mismatch faults and providing a remedial MPPT technique to suppress the mismatch, based on a temperature distribution analysis using a thermal camera.

Currently, thermal cameras are a useful tool for PV array fault diagnosis [20]–[29]. The health state of a grid-connected 20-kWp PV plant was investigated using a thermal camera [20]. It is effective in identifying breakdowns and hotspots but fails in distinguishing the different types of cell faults. Kaplani [21] studied the degradation of a PV system in the bus bars, contact solder bonds, blisters, and hotspots and also developed an algorithm to automatically differentiate faulty and healthy cells. Buerhopa *et al.* [22] reported the temperature differences for different faults such as bypassed substring, cell fracture, soldering, and shunted cell faults. Krenzinger and Andrade [24] investigated the thermal issues of the PV panel glass by developing an accurate temperature measurement method to offset reflection errors. Simon and Meyer [25] used infrared thermography to map the surface temperature distribution of a PV panel in a reverse bias mode in order to find the causes of localized heating. Kurnik *et al.* [26] derived an empirical coefficient for estimating the PV module temperature determined by analytical and experimental methods. However, in these papers, thermal cameras were only used independently to detect the temperature difference between cells or modules while captured image results are still open to human interpretation on whether or not the modules are faulty and how severe a fault may be.

In this study, thermal images are processed and input to a mathematical model for extracting quantitative information of a mismatch fault, which is then employed to regulate the MPPT control. This model combines electrical and thermal models through an energy balance based on a temperature distribution

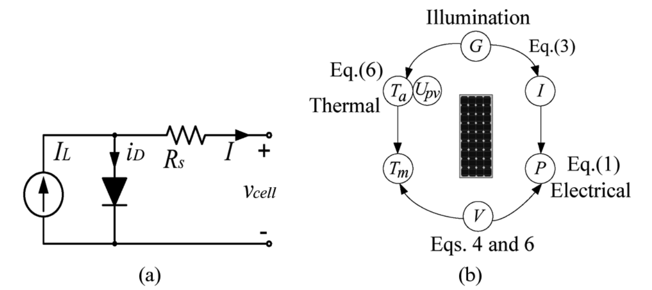

Fig. 2. Electrical and thermal characteristics of a PV cell. (a) Equivalent circuit [1]. (b) Energy balance.

analysis. After the temperature distribution characteristics are attained, the measured temperature difference can be evaluated, and a new MPPT scheme can be incorporated to minimize the impact of the occurred mismatch faults.

III. Modeling

When developing a parameter-based PV model, the electrical and thermal characteristics of the PV module should be included as they play an important role in the overall performance of PV systems. Fortunately, the electrical and thermal characteristics are interlinked through an energy balance that all receiving solar energy must be converted into electrical or heat energy.

A. Electrical Model

The electrical characteristic of a PV cell is influenced by both illumination and environmental temperature. The electrical model of a PV cell is generally represented by an equivalent circuit [see Fig. 2(a)] and is expressed by the following equations [10], [27]–[34]:

$$I = I_{\mathrm{L}} - I_{\mathrm{o}}\left[\exp\left(\frac{\varepsilon \cdot V}{T_m}\right) - 1\right] \tag{1}$$

$$\varepsilon = \frac{q}{N_s \cdot K \cdot A} \tag{2}$$

where

$$I_L = \frac{G}{G_{ref}}\left[I_{Lref} + k_i(T_m - T_{ref})\right] \tag{3}$$

$$I_o = I_{oref}\left(\frac{T_m}{T_{ref}}\right)^3 \exp\left[\frac{q \cdot E_{BG}}{N_s \cdot A \cdot K}\left(\frac{1}{T_{ref}} - \frac{1}{T_m}\right)\right] \tag{4}$$

where I is the PV module output current, I_L is the output current, q is the quantity of electric charge, A is the diode characteristic factor, K is the Boltzmann constant, I_o is the saturated current, T_m is the PV module temperature, G is the real irradiance of the PV cell, V is the output voltage, G_{ref} is the reference irradiance level (1000 W/m^2), I_{Lref} and I_{oref} are the reference values for I_L and I_o, and k_i is the current-temperature coefficient, normally provided by the manufacturer. T_{ref} is the reference temperature, N_s is the number of series-connected cells, and T_m is the PV module temperature. ε is a constant depending on q, N_s, K, A, and is calculated by the following equation:

$$I_{sc\_ref} - I_{mpp\_ref} = \frac{I_{sc\_ref}}{\exp\left(\frac{\varepsilon \cdot V_{oc\_ref}}{T_{ref}}\right) - 1}\left[\exp\left(\frac{\varepsilon \cdot V_{mpp\_ref}}{T_{ref}}\right) - 1\right] \quad (5)$$

where I_{mpp_ref}, I_{sc_ref}, and V_{oc_ref} are the MPP current, short-circuit current, and open-circuit voltage at a reference condition defined by the relevant standard.

B. Energy Balance

Energy balance can link electrical with thermal circuits based on two assumptions [32]: 1) the temperature difference between the PV cell and cover glass is neglected; 2) the cell temperature is uniform in a healthy module.

Therefore, the steady-state energy balance in PVs is given by

$$G \cdot A_m = V \cdot I + U_{pv} \cdot A_m(T_m - T_a) \quad (6)$$

where T_a is the ambient temperature, U_{pv} is an overall heat exchange coefficient from the module to ambient, and A_m is the PV panel area.

Equations (1) and (6) describe the electrical and thermal models, respectively, using main parameters such as I, V, T_m, G, U_{pv}, and T_a. Fig. 2(b) further illustrates the multiphysics loop of the energy balance in the PV system. The electrical parameters are mainly influenced by the effective solar energy S and module temperature T_m, whereas the thermal parameters are influenced by electrical power E and effective solar illumination G. Given a value of S, T_m depends on the electrical power of the PV module. As a result, this parameter-based model can be used to investigate the temperature difference upon a PV module fault.

IV. Temperature Distribution Analysis

When a mismatch fault occurs in the PV array, a temperature difference between the healthy and an unhealthy module is created, similar to partial shading observed from the terminal. Consequently, excessive heat and thermal stress can result in cell cracks. If the cell temperature exceeds its critical temperature, the delamination of cell encapsulants may occur. If the reverse bias exceeds the cell's breakdown voltage, the cell will be damaged [30]. In terms of the severity of mismatch faults, this paper defines three categories, namely, minor, medium, and heavy faults. Their terminal characteristics are different in the following aspects.

(i) Under a minor fault, the faulted power unit in the PV panel can still operate to generate electricity. As illustrated by the single arrow in Fig. 3(a), the current still passes through the PV cell string to generate an output. In this case, the faulty cell becomes an electrical load, powered by the healthy ones.

(ii) Under a medium fault, PV cells in the string are characterized by varying illumination levels. As presented in Fig. 3(b), the faulted cells can still operate as a source with a reduced power output. Because of the nonuniform illumination, the actual working point of the power unit is dictated by the operating point of the PV array.

(iii) Under a heavy-fault condition, the whole PV string is out of function while the bypass diode conducts to transmit the current, as indicated by the dotted arrow in Fig. 3(a). In essence, all PV cells in the string are open circuited.

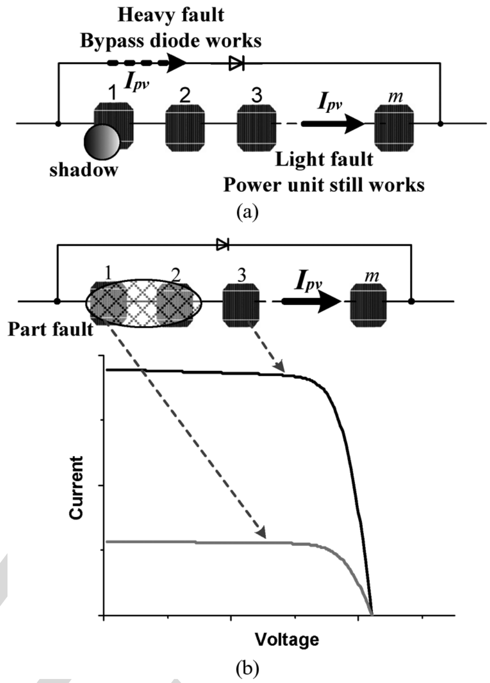

Fig. 3. Three categories of mismatch faults defined for a PV system. (a) Minor- and heavy-fault conditions. (b) Medium-fault condition.

If there exists a meaningful temperature difference, hotspot suppression is needed to shift the system MPP and to minimize the impact of the mismatch fault [35].

A. Analysis of Minor Faults

A temperature profile of the PV array under minor-fault conditions is presented in Fig. 4(a). The array is composed of b rows and a columns of PV modules where Module 21 is faulted. I_{array} and V_{array} are the current and voltage of the PV array, respectively. I_H and I_f are the currents of healthy and faulty strings, respectively. V_H is the module voltage of a healthy string, $V_{H'}$ is the voltage of the healthy module in the faulty string, T_H is the module temperature of a healthy string, $T_{H'}$ is the healthy module temperature within a faulted string, and T_f is the healthy cell temperature in a faulty power unit.

Under a minor-fault condition, the faulty PV cell cannot generate electricity and becomes a resistive load (R_{eq}). Owing to the series connection structure, the healthy cells supply power to the faulty PV cells (released as heat) and then create some hotspots. An equivalent circuit of the PV array is presented in Fig. 4(b), where V_{sf} stands for the voltage generated by the healthy PV cells in a faulty PV string, and R_{load} is the load resistance.

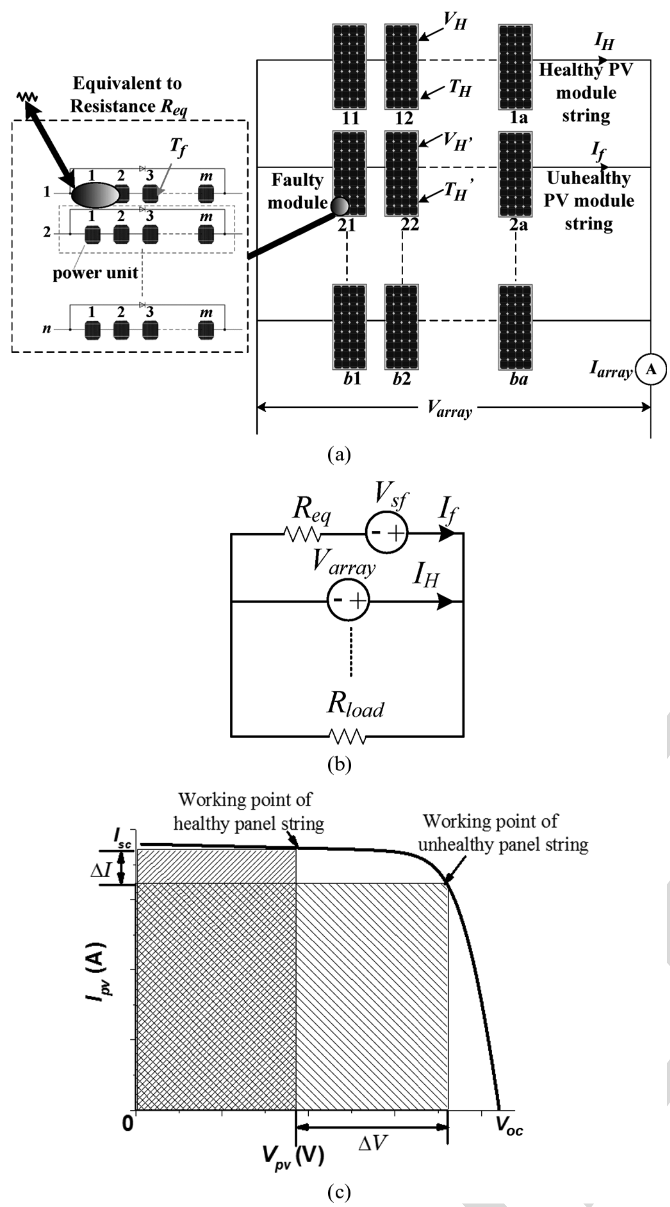

Fig. 4. PV system at a minor-fault condition. (a) PV array matrix. (b) Equivalent circuit upon a fault. (c) Shift of working points.

The electric characteristics of a faulty PV string are as follows:

$$V_{sf} - I_f R_{eq} = V_{array} \tag{7}$$

$$I_f = \frac{V_{sf}}{R_{eq} + R_{load}} \tag{8}$$

$$R_{eq} = \frac{V_{sf} - V_{array}}{I_f} \tag{9}$$

$$\Delta V = V_{H'} - V_H \tag{10}$$

$$\Delta I = I_H - I_f \tag{11}$$

$$I_f^2 \cdot R_{eq} < I_f (m - m_x) \frac{V_{H'}}{m \cdot n} \tag{12}$$

where ΔI is the current difference between the healthy and unhealthy strings, ΔV is the voltage difference between the healthy modules in healthy and unhealthy strings, and m_x is the number of faulty PV cells.

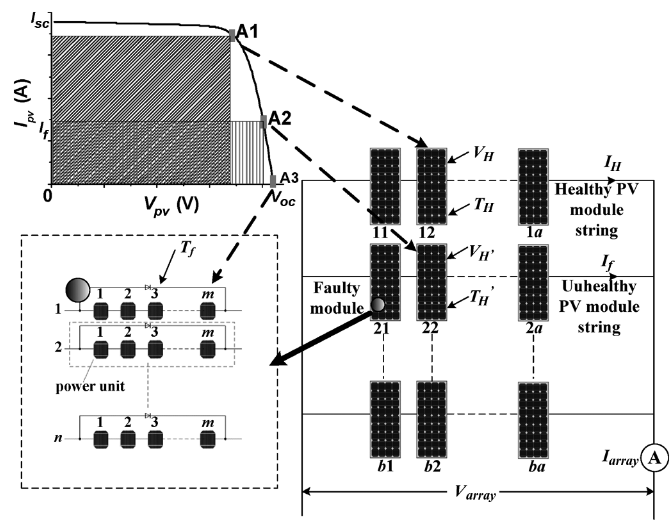

Fig. 5. PV system at a heavy-fault condition.

In Fig. 4(b), the voltage of a PV cell in a healthy string is lower than that of a healthy cell in a faulty string; the current of a PV cell in a healthy string is higher than that of a healthy cell in a faulty string. Equations (10)–(12) express the mathematical relationship for faulty and healthy PV strings. Equation (12) shows that when the output power of a faulted PV unit is higher than the I^2R power of its equivalent resistance, a minor fault is created, and hotspots begin to form on the fault cell.

Since the electrical power generated by healthy cells in the PV string supplies not only the load but also faulted cells (heating), the operating point in the current–voltage curve is effectively shifted. Fig. 4(c) demonstrates this in a PV system including healthy and unhealthy panel strings.

B. *Analysis of Heavy Faults*

Under a heavy-fault condition, the PV string containing the faulted cell/module loses production. Its operating points are illustrated in the output current–voltage curve in Fig. 5. Point A1 is the working point of the modules in the healthy string, A2 is the working point of the healthy modules in the faulty string, and A3 is the working point of healthy cells in the faulty module.

Because the faulty power unit is short-circuited by the bypass diode, the healthy cells in the faulty string are effectively open-circuited. The relative positions of A1, A2, and A3 are determined by the PV array structure and its electrical characteristics. Due to the antiparallel connection of the bypass diode, the faulty PV power unit is shorted by the diode. Therefore, its output voltage becomes zero. From (14), V_H is less than $V_{H'}$; I_H is greater than I_f, corresponding to working points A1 and A2. T_H and $T_{H'}$ depend on working points A1 and A2 in the curve. Because the faulty power unit is shorted by a bypass diode, the PV cells are open-circuited, corresponding to point A3. The output power of the faulted power unit is lower than the needed power of the equivalent resistance upon a fault; the power unit is shorted by the bypass diode.

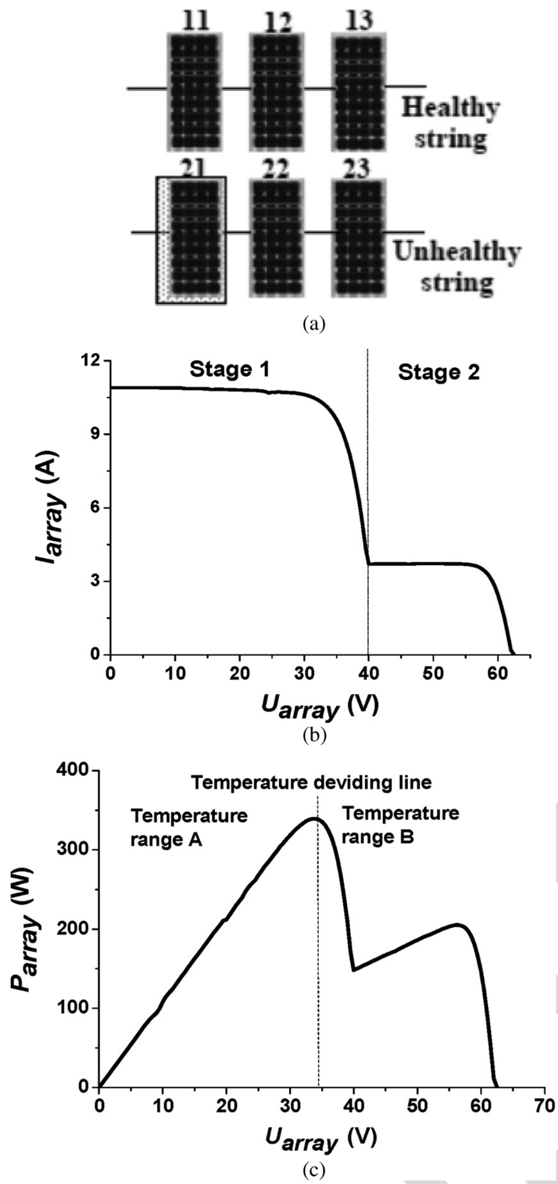

Fig. 6. PV system at a medium-fault condition. (a) Faulted module in a PV array. (b) Voltage–current curve of the faulted PV string. (c) Power–voltage curve of the faulted PV string.

V_H and $V_{H'}$ are thus given by

$$V_H = \frac{V_{array}}{a} \tag{13}$$

$$V_{H'} = \frac{V_H \cdot a \cdot n}{a \cdot n - n_x} \tag{14}$$

where n_x is the number of faulty power units in the faulty PV panel string, which can be identified by thermal cameras.

C. Analysis of Medium Faults

The operating point of the PV array strongly affects the condition of the healthy PV modules in the healthy string and sometimes in the fault string. Fig. 6(a) shows a 2 × 3 PV array under a medium fault, where module 21 is a faulted PV module,

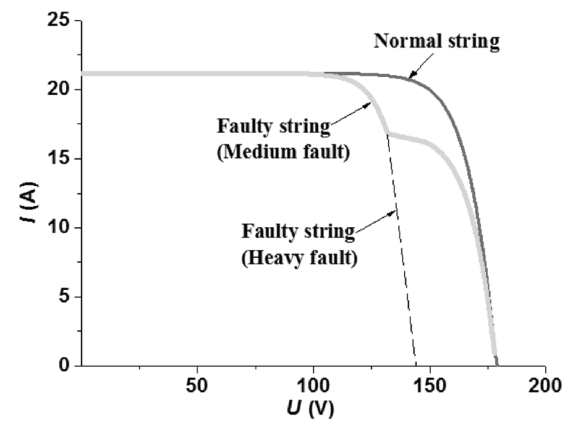

Fig. 7. Difference between medium and heavy faults.

and the rest of PV modules are healthy. Compared with other PV module (1000 W/m^2), No. 21 has the lower illumination (300 W/m^2). Fig. 6(b) and (c) presents the current–voltage and power–voltage curves, respectively, obtained from simulation.

In Fig. 6(b), the current–voltage curve of the PV array has a multistage feature, and the power–voltage curve has thus multiple MPPs. Two stages are identified in this figure. In Fig. 6(c), there exists a temperature dividing line in the power–voltage curve, separating two temperature ranges.

When the PV array works at stage 1, the current is between 4.5 and 10.8 A, and the corresponding voltage is 0–40 V. Both healthy and unhealthy strings can generate electricity. Since there are two healthy modules in the faulted string, they collectively provide an output voltage of 0–40 V. In the temperature range A, the temperature of modules 22 and 23 is lower than that of modules 11–13. According to the electrical and thermal balance equations, the output electrical power of the healthy modules in the faulty sting is higher than that of the healthy string. The corresponding temperature of the PV modules in the faulted string is lower than that in the healthy string.

While the PV array works at stage 2, the current is 0–4.5 A, and the corresponding voltage is 40–62 V. In this case, only the healthy string can generate electricity. The faulty string is shorted by the bypass diode, and the healthy module in the faulted string is in open circuit. In effect, all the effective solar energy is transferred into heat. In temperature range B, the faulted string has a higher temperature than the healthy string, indicating a different temperature characteristic to range A.

D. Terminal Characteristics of the Three Mismatch Faults

Based on a thermal image, PV array current and voltage information, three mismatch faults can be clearly identified.

A minor fault will cause hotspots characterized by a small faulty cell area (e.g., bird drops or leaves). When this fault occurs, it is easy to clear but often needs human intervention.

A medium fault and a heavy fault are both caused by nonuniform illumination. For the medium fault, the faulty PV string can still generate a high voltage output (140–180 V in Fig. 7). In the high-voltage region, the output current in the faulty string

TABLE I
SPECIFICATIONS OF THE EQUIPMENT

Item	Parameter	Value
PV Module	Open-circuit voltage	21.8 V
	Short-circuit current	6.23 A
	Power output	100 W
	MPP current	5.69 A
	MPP voltage	17 V
	Current temperature coefficient	0.06%/K
	Voltage temperature coefficient	–0.36%/K
	Power temperature coefficient	–0.45%/K
	NOCT	46±2
Thermal camera	Type	FLUKE Ti10
	IR resolution	160×120 pixels
	Thermal sensitivity (NETD)	< 0.13°C/130 mK
	Minimum focus distance	15 cm
	Spatial resolution (IFOV)	2.5 mRad
	Image frequency	9 Hz
	Accuracy	±2°C or 2%

is significantly lower than normal strings, whereas for the heavy fault, the faulty PV string is shorted so that it cannot generate any output. Therefore, the high-voltage region (140–180 V) is absent from the output curve in Fig. 7. Clearly, the medium and heavy faults can be easily distinguished. The medium and heavy faults would not cause an immediate damage to the PV module but can cause nonuniform aging and long-term damage to PV modules if left untreated.

V. EXPERIMENTAL TESTS

A PV experimental platform is developed using six PV panels arranged into two strings, with each having three series-connected PV panels, which are made of polysilicon and whose specifications are given in Table I. The PV panels' surface temperature is recorded by a *Fluke* thermal camera whose specifications are also listed in Table I.

The thermal camera can record a color image in varying intensities and send it to a central computer. In order to analyze the thermal feature of the device under test, the thermography of each PV panel is extracted by freehand cropping in a MATLAB program and is then used to calculate its relative temperature with a reference. Although the absolute accuracy of the thermal camera is only ±2 °C, its sensitivity is better than 0.1 °C. In this work, the proposed fault category analysis is based on identifying the temperature difference in the thermal image of the PV module and is thus effective.

Without a doubt, the use of thermal camera can help locate the faulty cells instantly and guide the maintenance work to conduct according to the type of occurred faults.

A. Tests Under a Minor Fault

Two parallel diodes are connected in the junction box, as shown in Fig. 8(a). One of the power units is connected with a resistance, and the other was made open-circuited to testify the temperature characteristics under different load conditions. Thus, there are two power units in all PV modules, each containing 18 PV cells.

The corresponding thermal image is presented in Fig. 8(b). The power unit A temperature is 32.6 °C, and the power unit B temperature is 36.1 °C. Because some of the solar energy in unit A is converted into electricity, its surface temperature is lower than that of unit B, in which all of the solar energy is transferred into heat.

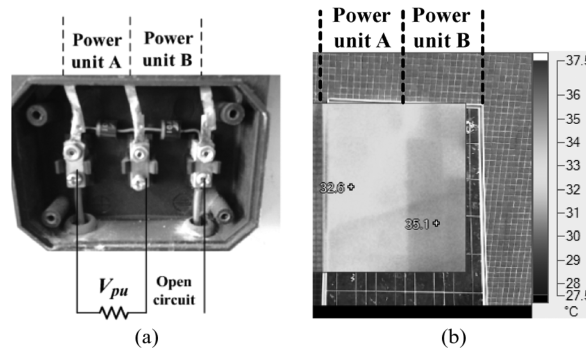

Fig. 8. Photos of the PV module. (a) Terminal connection. (b) Thermal image.

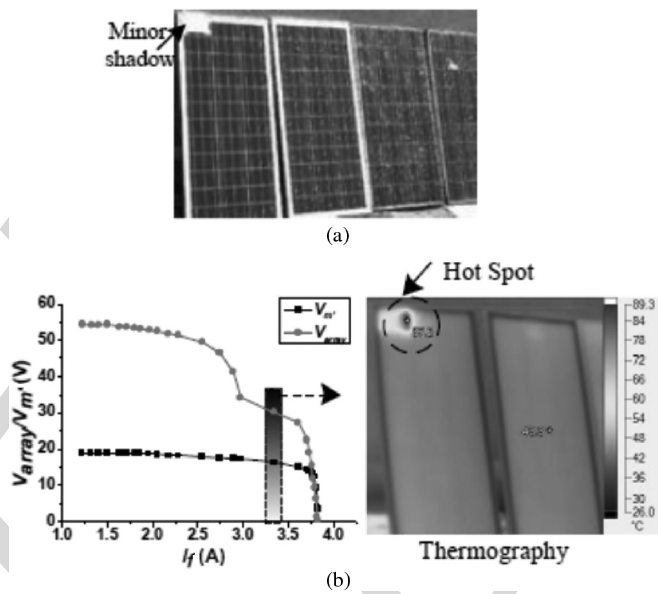

Fig. 9. Tests at a minor-fault condition. (a) Experimental scene to simulate minor shadowing. (b) Output characteristics and thermography.

Three PV panels are then connected in series, and one is covered by opaque materials to emulate partial shading. As shown in Fig. 9, a hotspot is recorded by thermography at the location of partial shading, and its I–V curve is shifted as well. A further experiment is carried out under 820-W/m^2 illumination at 25 °C ambient temperature. The terminal voltage is recorded 16 V from the faulty PV panel and 14 V from the two healthy panels. Because this is a minor shadow test, the healthy cells in the faulty string have a higher output voltage, and the faulted cell is equivalent to a resistance, raising the output voltage of the PV string under a minor-fault condition. From measurements, the voltage of the faulty PV cell is 9 V, and its equivalent resistance is 2.64 Ω. The electrical heating power for the faulty PV cell is 30.52 W, and the solar energy in the hotspot area is 15.5 W. According to the thermography measurement, the hotspot temperature reaches 87.2 °C, whereas the temperature of the healthy PV cells is only 44.3 °C. These are coincided with the theory analysis.

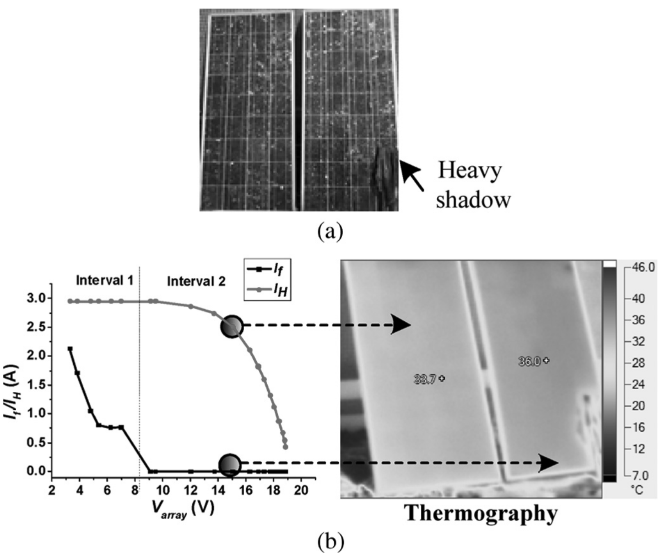

Fig. 10. Tests at a heavy-fault condition. (a) Experimental scene to simulate heavy shadowing. (b) Output characteristics and thermography.

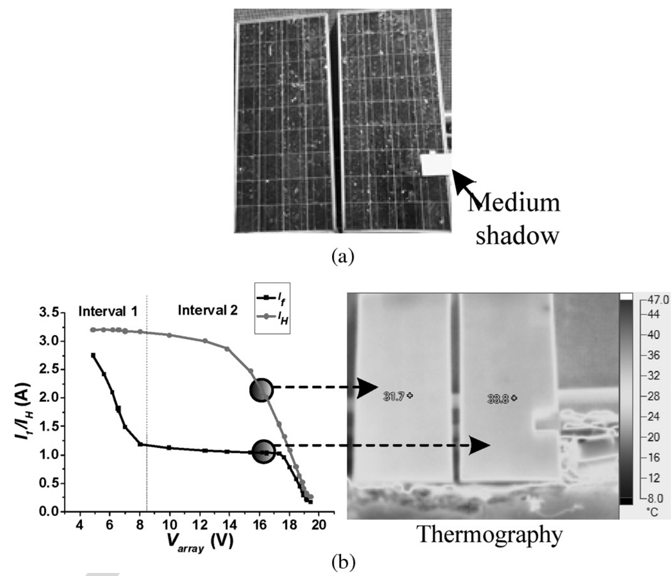

Fig. 11. Tests at a medium-fault condition. (a) Experimental scene to simulate medium shadowing. (b) Output characteristics and thermography.

B. Tests Under a Heavy Fault

Next, three PV cells are all covered up to create a heavy-fault condition, as shown in Fig. 10. Compared with the minor-fault scenario, the covered area is greater so that the faulted power unit is shorted by the bypass diode. The experiment is conducted under an illumination of 690 W/m^2 at 24 °C. The average temperature of the healthy PV panel is 33.7 °C, whereas the average temperature of the unhealthy PV module is 36.0 °C. The faulty PV panel is shorted by bypass diodes, and all the solar energy is converted into heat. However, the healthy PV panels are still capable of converting some of incoming solar energy into electricity, leading to a lower panel temperature. In Fig. 10, there is no current flowing at the faulted module during interval 2. Its current gradually increases during interval 1 because the faulty PV module is shorted by the bypass diode.

C. Tests Under a Medium Fault

In this test, one PV module is partially covered up by a thin paper to represent a medium-fault condition (e.g., partial shading), as shown in Fig. 11. The reason for using a thin paper is to ensure that some illumination can penetrate into the shaded cells through the paper. In the previous cases, light penetration is almost completely stopped.

The experiment is carried out under an illumination of 740 W/m^2 at 22 °C. The faulty power unit output is influenced by the unhealthy PV cells. The average temperature of a healthy PV panel is 31.7 °C, whereas that of the unhealthy PV module is recorded 33.8 °C. In interval 1, the faulty power unit is shorted by the bypass diode because the faulty power unit cannot generate a higher enough current to support load.

D. Tests Under Different Operating Points

Further tests are conducted to investigate the impact of the operating points, under a heavy-fault condition.

Fig. 12(a) shows the photo of a 2 × 3 PV array employed in this experiment. Fig. 12(b) and (c) depicts the output curves of the tested PV array. Fig. 12(d) shows a thermal image at working point A (with an array output voltage of 34 V). As discussed in Section III, the working point can cause the temperature difference. However, in this case, the two healthy modules in the fault string operate at 17 V, which is close to the MPP voltage. The corresponding temperatures are 19.9 °C and 19.8 °C, respectively, almost undistinguishable. The modules' output voltage in healthy string is 11.3 V, and the corresponding temperatures are 20.9 °C, 20.9 °C, and 21 °C for the three panels. At working point A, the module temperature in the healthy string is higher than the healthy module in the fault string. Fig. 12(e) shows a thermal image at working point B at the array output voltage 52 V. The output voltage of the healthy module is 17.3 V, which is close to MPP voltage, whereas the voltages of modules No. 22 and No. 23 are close to the open-circuit voltage, suggesting more energy is converted into heat. By the thermography measurement, the temperatures of healthy modules are 19.6 °C, 19.7 °C, and 19.7 °C, whereas the temperatures of healthy modules in the faulty string are both 21.6 °C. The temperature difference coincides with the theoretical analysis.

By the above analysis, it is clear that the temperatures of the healthy modules in both the healthy string and the unhealthy string are changed with the PV array output voltage. As a consequence, it is of critical importance to adjust the operating points according to different fault conditions.

E. Tests Under Open- and Short-Circuit Faults

Fig. 13 further compares the temperature difference between an open-circuit and a short-circuit scenario. At an open-circuit condition, the temperature distribution within a PV string is uniform; the corresponding temperature is 11.3 °C. Under a short-circuit condition, the temperature becomes varied. The

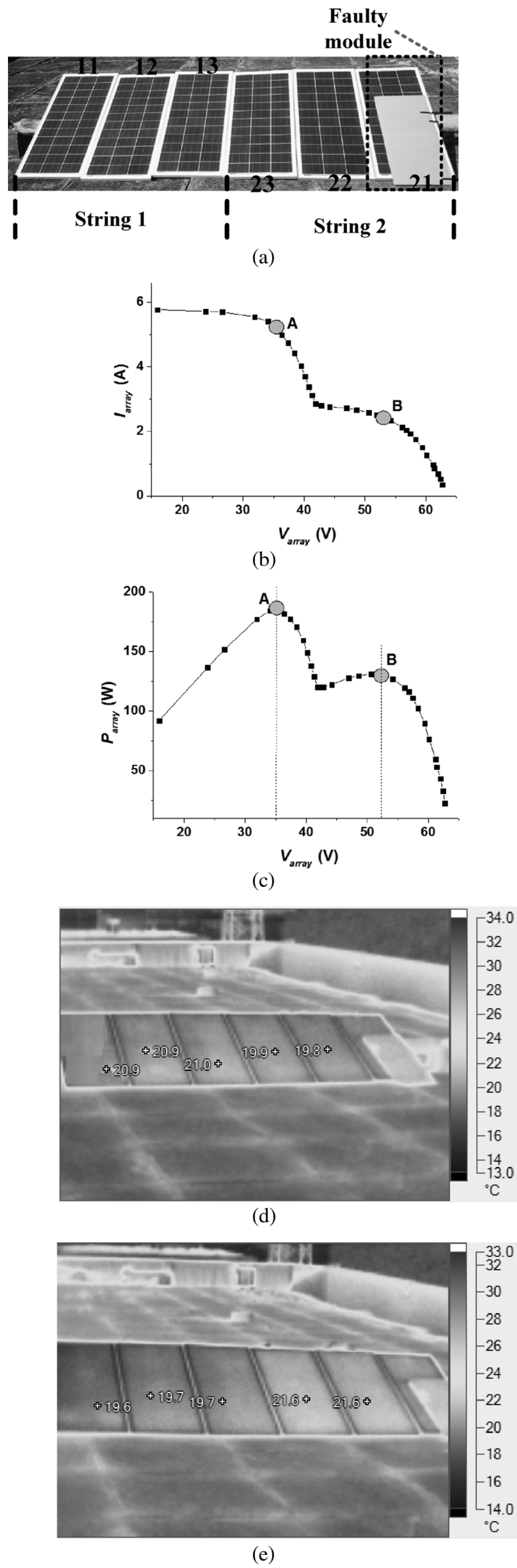

Fig. 12. Temperature distribution under two different operating points. (a) Tested PV panels. (b) Current–voltage curve. (c) Power–voltage curve. (d) Thermography at working point A. (e) Thermography at working point B.

temperatures of the faulty PV cells are 17.5 °C and 16.6 °C; the temperature of the healthy cells is 10.8 °C, which is even lower than that at the open-circuit condition. Under a short-circuit condition, the faulty PV cells have a higher equivalent resistance, thus shifting the working point of the healthy PV cells. The fault PV cell is heated up at the same time. Therefore, the healthy cells under a short-circuit fault have a lower temperature than that at an open-circuit fault.

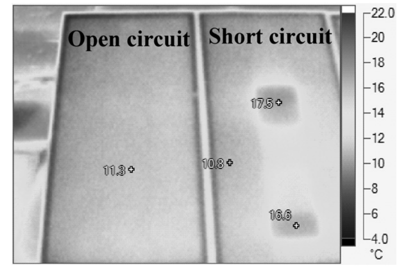

Fig. 13. Temperature difference between open and short circuits.

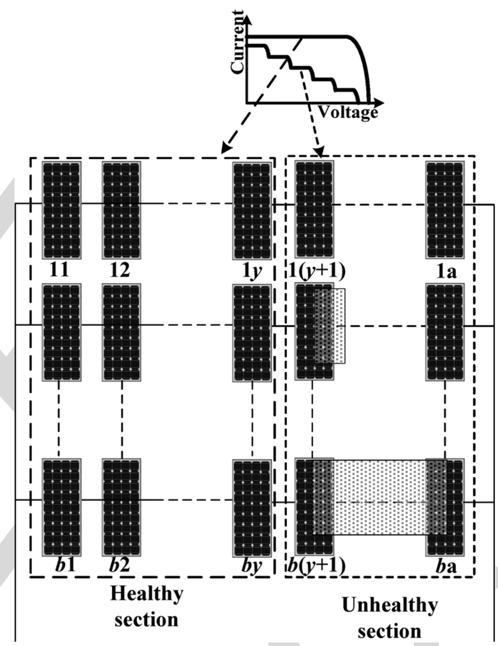

Fig. 14. Separation of healthy sections from fault PV arrays.

F. Assistance With MPPT Control

From the above analysis and experimental tests, the terminal characteristics and operating conditions of the PV module are known. The temperature distribution can then be input to the MPPT algorithm under mismatch fault conditions.

The maximum healthy section can be separated from fault PV arrays. As illustrated in Fig. 14, the whole PV array can be first divided into two sections: healthy and unhealthy. In the healthy section, all the modules in all strings are deemed to be fault free. That is, there is only an MPP in the section (local MPP). The global MPPT is effective to locate the first local MPP, significantly reducing the search range. In the unhealthy section where one or more modules are subject to shading, the temperature distribution of the faulty PV modules is then analyzed by thermography. As a result, the global MPP operating range can be directly located without much searching effort.

VI. Conclusion

Solar power is a cost-sensitive market. This work promotes its market acceptance by reducing the maintenance cost and improving the conversion efficiency of PV systems. This paper has presented a thermography-based temperature distribution analysis to analyze three different fault categories, and the proposed methodology was validated by both simulation and experimental test results. The proposed technology will lower the capital and operational costs of PV plants as well as increase their energy efficiency.

Compared with the existing methods, this work has made the following improvements.

(i) The thermal camera can help locate the faulty cells instantly and guide the maintenance work to conduct according to the type of occurred faults.

(ii) The temperature distributions under the PV fault conditions are analyzed by a new electrical–thermal model.

(iii) The mechanisms and impacts of three fault categories are defined and quantitatively studied. The mechanisms and difference of three faults is also illustrated.

(iv) The operating points of healthy and faulty PV arrays are described theoretically and experimentally, which could be used to improve the PV performance upon a mismatch fault.

(v) The thermography-based temperature distribution analysis is effective in establishing parameter-based models and developing an optimized global MPPT algorithm.

References

[1] A. Maki and S. Valkealahti, “Effect of photovoltaic generator components on the number of MPPs under partial shading conditions,” *IEEE Trans. Energy Convers.*, vol. 28, no. 4, pp. 1008–1017, Dec. 2013.

[2] M. Z. S. El-Dein, M. Kazerani, and M. M. A. Salama, “Optimal photovoltaic array reconfiguration to reduce partial shading losses,” *IEEE Trans. Sustainable Energy*, vol. 4, no. 1, pp. 145–153, Jan. 2013.

[3] E. V. Paraskevadaki and S. A. Papathanassiou, “Evaluation of MPP voltage and power of mc-Si PV modules in partial shading conditions,” *IEEE Trans. Energy Convers.*, vol. 26, no. 3, pp. 923–932, Sep. 2011.

[4] H. A. Lauffenburger and R. T. Anderson, “Reliability terminology and formulae for photovoltaic power systems,” *IEEE Trans. Rel.*, vol. R-31, no. 3, pp. 289–295, Aug. 1982.

[5] L. H. Stember, W. R. Huss, and M. S. Bridgman, “A methodology for photovoltaic system reliability and economic analysis,” *IEEE Trans. Rel.*, vol. R-31, no. 3, pp. 296–303, Aug. 1982.

[6] T. Takashima, J. Yamaguchi, K. Otani, K. Kato, and M. Ishida, “Experimental studies of failure detection methods in PV module strings,” in *Proc. 4th IEEE World Conf. Photovoltaic Energy Convers.*, 2006, vol. 2, pp. 2227–2230.

[7] Y. A. Mahmoud, W. Xiao, and H. H. Zeineldin, “A parameterization approach for enhancing PV model accuracy,” *IEEE Trans. Ind. Electron.*, vol. 60, no. 12, pp. 5708–5716, Dec. 2013.

[8] Y. H. Liu, S. C. Huang, J. W. Huang, and W. C. Liang, “A particle swarm optimization-based maximum power point tracking algorithm for PV systems operating under partially shaded conditions,” *IEEE Trans. Energy Convers.*, vol. 27, no. 4, pp. 1027–1035, Dec. 2012.

[9] K. Ding, X. Bian, H. Liu, and T. Peng, “A MATLAB–Simulink-based PV module model and its application under conditions of nonuniform irradiance,” *IEEE Trans. Energy Convers.*, vol. 27, no. 4, pp. 864–872, Dec. 2012.

[10] A. Mäki and S. Valkealahti, “Power losses in long string and parallel-connected short strings of series-connected silicon-based photovoltaic modules due to partial shading conditions,” *IEEE Trans. Energy Convers.*, vol. 27, no. 1, pp. 173–183, Mar. 2012.

[11] T. Takashima *et al.*, “Experimental studies of fault location in PV module strings,” *Sol. Energy Mater. Sol. Cells*, vol. 93, no. 6/7, pp. 1079–1082, Jun. 2009.

[12] H. Patel and V. Agarwal, “MATLAB-based modeling to study the effects of partial shading on PV array characteristics,” *IEEE Trans. Energy Convers.*, vol. 23, no. 1, pp. 302–310, Mar. 2008.

[13] H. Patel and V. Agarwal, “Maximum power point tracking scheme for PV systems operating under partially shaded conditions,” *IEEE Trans. Ind. Electron.*, vol. 55, no. 4, pp. 1689–1698, Apr. 2008.

[14] H. Ziar, M. Nouri, B. Asaei, and S. Farhangi, “Analysis of overcurrent occurrence in photovoltaic modules with overlapped by-pass diodes at partial shading,” *IEEE J. Photovoltaics*, vol. 4, no. 2, pp. 713–721, Mar. 2014.

[15] A. Bidram, A. Davoudi, and R. S. Balog, “Control and circuit techniques to mitigate partial shading effects in photovoltaic arrays,” *IEEE J. Photovoltaics*, vol. 2, no. 4, pp. 532–546, Oct. 2012.

[16] E. I. Batzelis, I. A. Routsolias, and S. A. Papathanassiou, “An explicit PV string model based on the Lambert W function and simplified MPP expressions for operation under partial shading,” *IEEE Trans. Sustainable Energy*, vol. 5, no. 1, pp. 301–312, Jan. 2014.

[17] E. Karatepe and T. Hiyama, “Simple and high-efficiency photovoltaic system under non-uniform operating conditions,” *IET Renew. Power Gen.*, vol. 4, no. 4, pp. 354–368, Jul. 2010.

[18] B. N. Alajmi, K. H. Ahmed, S. J. Finney, and B. W. Williams, “Maximum power point tracking technique for partially shaded photovoltaic systems in microgrids,” *IEEE Trans. Ind. Electron.*, vol. 60, no. 4, pp. 1596–1606, Apr. 2013.

[19] L. F. L.Villa, T. P. Ho, J. C. Crebier, and B. Raison, “A power electronics equalizer application for partially shaded photovoltaic modules,” *IEEE Trans. Ind. Electron.*, vol. 60, no. 3, pp. 1179–1190, Mar. 2013.

[20] G. Acciani, G. B. Simione, and S. Vergura, “Thermographic analysis of photovoltaic panels,” in *Proc. ICREPQ*, Granada, Spain, 2010, pp. 1–3.

[21] E. Kaplani, “Detection of degradation effects in field-aged c-Si solar cells through IR thermography and digital image processing,” *Int. J. Photoenergy*, vol. 2012, pp. 396 792-1–396 792-11, 2012.

[22] C. L. Buerhopa *et al.*, “Reliability of IR-imaging of PV-plants under operating conditions,” *Sol. Energy Mater. Sol. Cells*, vol. 107, pp. 154–164, Dec. 2012.

[23] P. Parinya, B. Wiengmoon, D. Chenvidhya, and C. Jivacate, “Comparative study of solar cells characteristics by temperature measurement,” in *Proc. 22nd Eur. Photovoltaic Sol. Energy Conf.*, Milan, Italy, 2007, pp. 2775–2778.

[24] A. Krenzinger and A. C. Andrade, “Accurate outdoor glass thermographic thermometry applied to solar energy devices,” *Sol. Energy*, vol. 81, no. 8, pp. 1025–1034, Aug. 2007.

[25] M. Simon and E. L. Meyer, “Detection and analysis of hot-spot formation in solar cells,” *Sol. Energy Mater. Sol. Cells*, vol. 94, no. 2, pp. 106–113, Feb. 2010.

[26] J. Kurnik, M. Jankovec, K. Brecl, and M. Topic, “Outdoor testing of PV module temperature and performance under different mounting and operational conditions,” *Sol. Energy Mater. Sol. Cells*, vol. 95, no. 1, pp. 373–376, Jan. 2011.

[27] G. Farivar and B. Asaei, “A new approach for solar module temperature estimation using the simple diode model,” *IEEE Trans. Energy Convers.*, vol. 26, no. 4, pp. 1118–1126, Dec. 2011.

[28] M. U. Siddiqui, A. F. M. Arif, L. Kelley, and S. Dubowsky, “Three-dimensional thermal modeling of a photovoltaic module under varying conditions,” *Sol. Energy*, vol. 86, no. 9, pp. 2620–2631, Sep. 2012.

[29] H. F. Tsai and H. L. Tsai, “Implementation and verification of integrated thermal and electrical models for commercial PV modules,” *Sol. Energy*, vol. 86, no. 1, pp. 654–665, Jan. 2012.

[30] E. L. Meyer and E. E. van Dyk, “Assessing the reliability and degradation of photovoltaic module performance parameters,” *IEEE Trans. Rel.*, vol. 53, no. 1, pp. 83–92, Mar. 2004.

[31] A. Chatterjee, A. Keyhani, and D. Kapoor, “Identification of photovoltaic source models,” *IEEE Trans. Energy Convers.*, vol. 26, no. 3, pp. 883–889, Sep. 2011.

[32] M. Mattei, G. Notton, C. Cristofari, M. Muselli, and P. Poggi, “Calculation of the polycrystalline PV module temperature using a simple method of energy balance,” *Renew. Energy*, vol. 31, no. 4, pp. 553–567, Apr. 2006. AQ1

[33] A. Luque, G. Sala, and J. C. Arboiro, “Electric and thermal model for non-uniformly illuminated concentration cells,” *Sol. Energy Mater. Sol. Cells*, vol. 51, no. 3/4, pp. 269–290, Feb. 1998.

[34] Y. Hu *et al.*, “Photovoltaic fault detection using a parameter based model,” *Sol. Energy*, vol. 96, pp. 96–10, Oct. 2013.

[35] S. A. Spanoche, J. D. Stewart, S. L. Hawley, and I. E. Opris, “Model-based method for partially shaded PV module hot-spot suppression,” *IEEE J. Photovoltaics*, vol. 3, no. 2, pp. 785–790, Apr. 2013.

Yihua Hu (M'13) received the B.S. degree in electrical motor drives and the Ph.D. degree in power electronics and drives from China University of Mining and Technology, Jiangsu, China, in 2003 and 2011, respectively.

Between 2011 and 2013, he was a Postdoctoral Fellow with the College of Electrical Engineering, Zhejiang University, Hangzhou, China. Between November 2012 and February 2013, he was an academic Visiting Scholar with the School of Electrical and Electronic Engineering, Newcastle University, Newcastle upon Tyne, U.K. He is currently a Research Associate with the Department of Electronic and Electrical Engineering, University of Strathclyde, Glasgow, U.K. His research interests include photovoltaic generation systems, dc–dc/dc–ac converters, and electrical motor drives.

Wenping Cao (M'05–SM'11) received the B.Eng. degree in electrical engineering from Beijing Jiaotong University, Beijing, China, in 1991 and the Ph.D. degree in electrical machines and drives from the University of Nottingham, Nottingham, U.K., in 2004.

He is currently a Senior Lecturer with Queen's University Belfast, Belfast, U.K. His research interests include thermal performance of electric machines, drives, and power electronics.

Dr. Cao was a recipient of the Best Paper Award at the LDIA'13 Conference. He serves as an Associate Editor for the IEEE TRANSACTIONS ON INDUSTRY APPLICATIONS, the *IEEE Industry Applications Magazine*, the *IET Power Electronics*, and nine other international journals. He is also a member of the Institution of Engineering and Technology and a Fellow of Higher Education Academy.

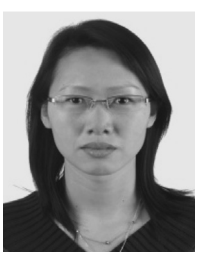

Jien Ma received the B.Eng. degree in mechatronics from Yanshan University, Qinhuangdao, China, in 2003 and the Ph.D. degree in electromechanics from Zhejiang University, Hangzhou, China, in 2009.

She is currently a Lecturer with the College of Electrical Engineering, Zhejiang University. Her interests include electrical machines and drives, including permanent-magnet machines and cooling system design, mechatronics machines, and magneto fluid bearings.

Stephen J. Finney received the M.Eng. degree in electrical and electronic engineering from Loughborough University of Technology, Loughborough, U.K., in 1988 and the Ph.D. degree from Heriot-Watt University, Edinburgh, U.K., in 1995.

Prior to joining the Power Electronics Research Group at Heriot-Watt University in 1990, he was with the Electricity Council Research Centre. From 1994 to 2005, he was a member of the academic staff with Heriot-Watt University. Since 2005, he has been with the Institute of Energy and Environment, University of Strathclyde, Glasgow, U.K., where he is currently a Professor, specializing in power electronic systems. His research interests include power electronics for high-power applications and the use of power electronics for power transmission and distribution.

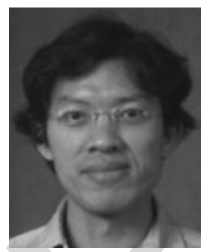

David Li received the Ph.D. degree in electrical engineering from National Taiwan University, Taipei, Taiwan, in 2001.

He then joined the Industrial Technology Research Institute, Taiwan, and the University of Edinburgh, Edinburgh, U.K., working on optical communications and optoelectronics. Since January 2014, he has been a Senior Lecturer with the Centre for Biophotonics, University of Strathclyde, Glasgow, U.K. His current research interests include solid-state cameras, embedded systems, digital signal processing, mixed-signal integrated circuit design, fluorescence-based sensing and imaging systems, electrical impedance sensing systems, forward models of electrical impedance tomography, and finite-element/finite-difference and numerical modeling.

AUTHOR QUERIES

AUTHOR PLEASE ANSWER ALL QUERIES

AQ1 = Note that references [32] and [35] are the same. Therefore, reference [35] was deleted from the list. Citations were renumbered accordingly. Please check.

END OF ALL QUERIES